The (Metal–Metal)-Nonbonding $[Fe_2(CO)_6(\mu_2\text{-}PPh_2)_2]^{2-}$ Dianion. Synthesis, Structural Analysis of Its Unusual Dimeric Geometry, and Stereochemical-Bonding Implications

Robert E. Ginsburg,[1a] Richard K. Rothrock,[1b,c] Richard G. Finke,[1b,d] James P. Collman,[1b] and Lawrence F. Dahl*[1a]

Contribution from the Departments of Chemistry, University of Wisconsin—Madison, Madison, Wisconsin 53706, and Stanford University, Stanford, California 94305.
Received January 22, 1979

Abstract: The $[Fe_2(CO)_6(\mu_2\text{-}PPh_2)_2]^{2-}$ dianion, which reacts with alkyl halides to yield (upon protonation) aldehydes in quantitative yield, was prepared as $Na_2[Fe_2(CO)_6(\mu_2\text{-}PPh_2)_2]\cdot 5THF$ from the reduction with sodium dispersion in THF of the corresponding neutral dimer (for which a cyclic voltammogram in acetonitrile solution exhibits a single two-electron reversible reduction wave). Suitable crystals for an X-ray diffraction investigation of this burgundy-red dianion were finally obtained as the $[Na(2,2,2\text{-crypt})]^+$ salt. Its centrosymmetrically required geometry containing a strictly planar Fe_2P_2 core is best described as being formally comprised of two distorted trigonal bipyramids which share a common axial-equatorial edge: this edge-bridged bi(trigonal-bipyramidal) architecture is uncommon in that there are only a few other crystallographically known examples of a five-coordinate metal dimer without a metal–metal bond. A geometrical comparison of this dianion with its neutral diphenylphosphido-bridged parent reveals that a dramatic change in configuration has taken place upon reduction of the (Fe–Fe)-bonded $Fe_2(CO)_6(\mu_2\text{-}PPh_2)_2$ molecule due to cleavage of the electron-pair Fe–Fe bond. A complete flattening of the highly bent Fe_2P_2 core is found to occur which increases the Fe–Fe distance from a bonding value of 2.623 (2) Å in the parent molecule to a nonbonding value of 3.630 (3) Å in the dianion. This structural study of the dianion of a representative member of the well-known (metal–metal)-bonded $Fe_2(CO)_6(\mu_2\text{-}X)_2$ series furnishes the first experimentally definitive evidence that electron occupation of the lowest unoccupied molecular orbital (i.e., LUMO) of the corresponding neutral parent completely ruptures the metal–metal bond, in agreement with previous molecular orbital calculations which showed that the LUMOs of these neutral dimers possess large antibonding dimetal orbital character. Its structural features are correlated with spectroscopic data for this class of dimers, and the resulting bonding and stereochemical implications are discussed. The finding that the metal–metal distance can increase by as much as 1.0 Å upon a two-electron reduction strikingly emphasizes the importance of the "net" metal–metal interactions in dictating the resultant geometry of a metal cluster. $[Na(2,2,2\text{-crypt})]_2^+[Fe_2(CO)_6(\mu_2\text{-}PPh_2)_2]^{2-}$ crystallizes in a triclinic unit cell of $P\bar{1}$ symmetry with lattice constants of a = 12.466 (6) Å, b = 16.861 (6) Å, c = 10.797 (4) Å, α = 127.92 (2)°, β = 84.04 (2)°, and γ = 101.83 (3)°; ρ_{calcd} = 1.37 g/cm³ for Z = 1. Least-squares refinement gave $R_1(F)$ = 7.9% and $R_2(F)$ = 7.8% for 2681 independent diffractometry data with $I \geq 2.0\sigma(I)$.

Introduction

Interest in aryl and alkyl phosphido- and mercapto-bridged organometallic clusters has recently been renewed, as exemplified (1) by the report of Collman et al.[2] on the reduction of $Fe_2(CO)_6(\mu_2\text{-}PPh_2)_2$ to the dianion and its subsequent reaction with alkyl halides to yield, upon protonation, aldehydes in quantitative yield;[2] (2) by the report of Ryan, Pittman, and O'Connor[3] on the demonstrated ability of $Co_4(CO)_8(\mu_2\text{-}CO)_2(\mu_4\text{-}PPh)_2$[4] as a hydroformylation catalyst; (3) by the report of Poilblanc[5] on the use of mercapto-bridged metal dimers to activate substrates such as H_2 by oxidative addition on two initially nonbonding metal sites which concomitantly form a metal–metal bond as part of the reaction's driving force.

The work of Collman and co-workers[2] again focused attention on the influence of valence electrons on the geometry of a $Fe_2(CO)_6(\mu_2\text{-}X)_2$ dimer (Figure 1) upon reduction of the neutral species. Their preparation of the $[(Fe_2(CO)_6(\mu_2\text{-}PPh_2)_2]^{2-}$ dianion and its isolation as a red crystalline salt of composition $Na_2[Fe_2(CO)_6(\mu_2\text{-}PPh_2)_2]\cdot 5THF$ offered the hope that an X-ray crystallographic investigation could be carried out. Such a structural characterization of the dianion was deemed to be exceedingly important in correlating its geometry and electronic configuration with those of the structurally known neutral parent,[6] especially since it has been previously shown by Teo et al.[7] from nonparametrized MO calculations, based on the observed (Fe–Fe)-bonded distance for the neutral $Fe_2(CO)_6(\mu_2\text{-}PPh_2)_2$ dimer and an assumed (Fe–Fe)-nonbonded geometry for the model $[Fe_2(CO)_6(\mu_2\text{-}PH_2)_2]^{2-}$ dianion, that the Fe–Fe bond was broken upon reduction by an addition of two electrons to a MO of highly antibonding bimetallic character (in both the neutral dimer and the dianion). A direct comparison of structural features between the neutral parent and its reduced offspring was needed not only to substantiate the theoretical predictions but also to provide an unequivocal operational test of the presumed importance of Fe–Fe bonding in a representative $Fe_2(CO)_6(\mu_2\text{-}X)_2$ dimer. Before its present unambiguous solution, this problem had been unresolved in our laboratories for 15 years.

During the course of the successful use by Collman et al.[2] of the presumed (metal–metal)-nonbonded $[Fe_2(CO)_6(\mu_2\text{-}PPh_2)_2]^{2-}$ dianion to produce, upon alkylation, acyl dimeric monoanions via alkyl migration with concomitant formation of the metal–metal bond, a collaborative effort was undertaken to obtain a crystallographic analysis of the dianion. Since their isolated $Na_2[Fe_2(CO)_6(\mu_2\text{-}PPh_2)_2]\cdot 5THF$ salt did not yield suitable X-ray diffraction data, attempts made in both laboratories to replace the Na^+ counterion with other larger counterions finally culminated in the isolation by Rothrock of the $[Na(2,2,2\text{-crypt})]_2^+[Fe_2(CO)_6(\mu_2\text{-}PPh_2)_2]^{2-}$ salt and its structural determination. The resulting stereochemical information presented here has provided a requisite basis for a further elucidation of the electronic and geometric interrelationship of the $Fe_2(CO)_6X_2$-type dimer upon reduction.

Experimental Section

Preparation and Characterization of $[Na(2,2,2\text{-crypt})_2^+(Fe_2(CO)_6(\mu_2\text{-}PPh_2)_2]^{2-}$. In an inert atmosphere box, either orange, crystalline $Fe_2(CO)_6(\mu_2\text{-}PPh_2)_2\cdot 1.0C_6H_6$ (analyzed by NMR) or yellow powder $Fe_2(CO)_6(\mu_2\text{-}PPh_2)_2$ was dissolved in THF and treated with

0002-7863/79/1501-6550$01.00/0

a stoichiometric amount of sodium (50% dispersion). After being stirred overnight at room temperature, the product, $Na_2[Fe_2(CO)_6(\mu_2\text{-}PPh_2)_2]\cdot 5THF$, was crystallized by a slow addition of hexane. Its IR spectrum in THF solution showed absorption bands in the carbonyl region at 1930 (m), 1905 (vs), 1845 (vs), 1825 (s), and 1800 (vs) cm^{-1}. Anal. Calcd for $C_{50}H_{60}Fe_2P_2Na_2$: C, 56.83; H, 5.72; Fe, 10.57; P, 5.86; Na, 4.35. Found: C, 56.66; H, 5.50; Fe, 10.77; P, 5.94; Na, 4.32.

Deep burgundy-red crystals of $[Na(2,2,2\text{-crypt})]_2^+[Fe_2(CO)_6(\mu_2\text{-}PPh_2)_2]^{2-}$ were obtained by vapor diffusion of hexane into a solution of dry NMP (viz., *N*-methyl-2-pyrrolidone) containing a 1:2 molar ratio of $Na_2[Fe_2(CO)_6(\mu_2\text{-}PPh_2)_2]\cdot 5THF$ and 2,2,2-crypt (viz., $N(C_2H_4OC_2H_4OC_2H_4)_3N$). A KBr-pellet IR spectrum showed carbonyl bands at 1920 (w, sh), 1890 (vs), 1833 (vs, br), and 1805 (vs, br) cm^{-1}. Solution IR or NMR spectra were not obtained owing to the insolubility of this salt (even in NMP, THF, and Me_2SO). Anal. Calcd for $C_{66}H_{92}Fe_2N_4Na_2P_2O_{18}$: C, 54.70; H, 6.40; Fe, 7.71; N, 3.87; Na, 3.17. Found: C, 54.44; H, 6.59; Fe, 7.58; N, 3.90; Na, 3.03.

X-ray Crystallographic Study. A suitable crystal of approximate dimensions 0.20 × 0.20 × 0.30 mm was mounted under an argon atmosphere inside a thin-walled Lindemann glass capillary. This crystal was accurately centered optically on a computer-controlled four-circle Syntex $P\bar{1}$ diffractometer equipped with a scintillation counter, a pulse height analyzer adjusted to admit 90% of the Mo $K\bar{\alpha}$ ($\lambda\alpha_1$ = 0.709 30 Å, $\lambda\alpha_2$ = 0.713 59 Å), and a crystal graphite monochromator set at a Bragg 2θ angle of 12.2°. Fifteen reflections selected from a rotation photograph were centered automatically and used in a least-squares refinement to align the crystal and determine an orientation matrix from which angular settings for each reflection were generated. In order to obtain precise latter constants and a more reliable orientation matrix, preliminary data were sampled between 15 and 20° in 2θ for only those peaks whose net intensity was greater than 150 counts. Fifteen peaks so identified were used in a least-squares refinement and redetermination of the lattice constants and orientation matrix, which were subsequently used in the actual data collection. The triclinic cell dimensions recorded at the ambient laboratory temperature of 22 °C are a = 12.466 (6) Å, b = 16.861 (6) Å, c = 10.797 (4) Å, α = 127.92 (2)°, β = 84.04 (2)°, and γ = 101.83 (3)°. The cell volume of 1751 (1) Å^3 containing one $[Na(2,2,2\text{-crypt})]_2^+[Fe_2(CO)_6(\mu_2\text{-}PPh_2)_2]^{2-}$, which corresponds to $F(000)$ = 1160, gives a calculated density of 1.37 g/cm^3. Intensities of the triclinic reciprocal lattice were sampled once over the independent octants hkl, $h\bar{k}l$, $hk\bar{l}$, $h\bar{k}\bar{l}$ within the 2θ data range of 3.0–50.0°. The θ–2θ scan technique was utilized with a variable scan speed of 2.00–24.00°/min in 2θ. It was not necessary to obtain the background at both extremes of each scan because of the recent availability of a data-reduction program[8a] which performs a profile analysis on the step scans of a diffracted reflection. The scan speed and width for an individual diffraction maximum were determined by its relative peak intensity. Two standard reflections, remeasured after every 48 data reflections, showed no intensity variations greater than 3% during the entire data collection. The data were reduced and corrected for polarization of the incident beam due to the crystal monochromator and variable scan speed by use of the program CARESS.[8a] The 4916 measured data were merged[8b] to yield 4619 independent reflections, of which 2681 were considered observed with $I > 2.0\sigma(I)$. No absorption corrections[8c] were applied in that the range of transmission coefficients, based on a calculated linear absorption coefficient[9a] of 5.27 cm^{-1}, varied from only 0.88 to 0.90.

Structural Determination and Refinement. The atomic scattering factors of Cromer and Mann[9b] for the nonhydrogen atoms and Stewart et al.[9c] for the hydrogen atoms were used in all structure-factor calculations. Anomalous dispersion corrections[9d] were applied to the scattering factors of Fe, P, and Na.

The structure was solved under assumed centrosymmetric $P\bar{1}$ symmetry by direct methods[10] with the program MULTAN.[8d] Normalized structure factors, $|E|$'s, were calculated,[10] and the 400 highest $|E|$'s with $|E| > 1.8$ and the 50 lowest $|E|$'s were used as input data. The starting set for the phase determination was comprised of three origin-defining reflections and five general reflections. Of the resulting 32 generated phase sets, the one which provided the correct solution for the crystal structure had an absolute figure of merit of 1.293, a ψ-zero figure of merit of 525.7, a residual index of 12.27, and a combined figure of merit of 2.177 (based on the individual components weighted at 0.8, 1.2, and 1.0, respectively). A Fourier synthesis[8e] phased on the E's from this solution revealed the independent iron and phosphorus atom of the dianion along with the sodium, two nitrogen, and four oxygen atoms of the independent $[Na(2,2,2\text{-crypt})]^+$ cation. A Fourier synthesis[8e] phased on these atoms gave an initial R_1 = 43.4%. Successive Fourier and difference Fourier syntheses revealed the positions for all the nonhydrogen atoms. Block-diagonal least-squares refinement[8f] of the positional parameters and isotropic temperature factors of all atoms converged at R_1 = 10.76% and R_2 = 11.18%. Continued block-diagonal least squares with anisotropic temperature factors utilized for all nonhydrogen atoms converged at R_1 = 9.06% and R_2 = 9.39%.

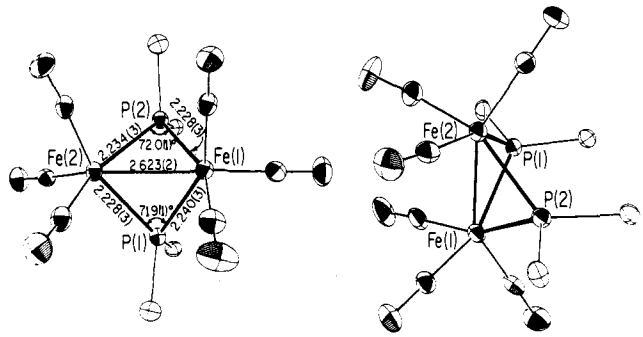

Figure 1. Two views of the neutral $Fe_2(CO)_6(\mu_2\text{-}PPh_2)_2$ parent (with phenyl rings removed for clarity). This representative $Fe_2(CO)_6(\mu_2\text{-}X)_2$-type dimer, formally arising from the junction of the basal planes of two tetragonal pyramids along the common P···P line, has a highly nonplanar Fe_2P_2 core (with a torsional angle θ = 100.0°) containing sharply acute bridging angles of 72.0° (av) and an electron-pair Fe–Fe bond of 2.623 (2) Å. The $Fe_2(CO)_6P_2$ fragment closely conforms to C_{2v} symmetry.

At this point hydrogen coordinates were idealized[8g] on the phenyl rings and on the methylene carbon atoms of the cryptate. Subsequent block-diagonal least-squares refinement of the positional parameters and anisotropic thermal coefficients was performed to convergence followed by full-matrix refinement in which only the positional parameters of the nonhydrogen atoms were varied. In these refinements coordinates and temperature factors of the hydrogen atoms were held constant, but new idealized hydrogen coordinates were recalculated from the resulting new coordinates of the nonhydrogen atoms after every third least-squares cycle. Convergence of the full-matrix refinement[8h] occurred after the second cycle with discrepancy indices for the 2681 independent reflections of R_1 = 7.94% and R_2 = 7.79% and with no shift-over-error ratio, Δ/σ, greater than 0.05. A final difference Fourier map, which had no residual peak greater than 0.78 e$^-$/A^3, revealed no unusual features.

The positional and thermal parameters from the final cycle of the full-matrix least-squares refinement are given in Table I. Interatomic distances and bond angles with esd's calculated from the Busing-Martin-Levy ORFFE program[8i] are presented in Table II, which also lists dehedral angles for the $[Na(2,2,2\text{-crypt})]^+$ cation. Selected least-squares planes[8j] and interplanar angles are given in Table III. All figures were computer drawn with the thermal ellipsoid plotting program written by Johnson.[8k] The observed and calculated structure factors are given as supplementary material.

Results and Discussion

General Description of the Crystal Structure. The solid-state structure is composed of discrete monocations and dianions (Figures 2 and 3). The complete encapsulation of the Na^+ ion by the cryptate ligand (Figure 4) effectively prevents the formation of any ion pairing. The monocations and dianions are well separated in the unit cell (Figure 5) with no interionic nonhydrogen contacts less than 3.5 Å. Hence, there is no evidence of unusual packing forces which would produce marked geometric distortions of either the monocations or dianions.

$[Fe_2(CO)_6(\mu_2\text{-}PPh_2)_2]^{2-}$ Dianion. A. Previously Determined Stereochemical and Bonding Properties of the $Fe_2(CO)_6X_2$-Type Dimer and Its Anions. Structural and bonding studies of $Fe_2(CO)_6X_2$ dimers containing Fe_2E_2-bridged cores (where E denotes the metal-attached bridging atom of ligand X) commenced in our laboratories in 1963 with a crystallographic determination by Dahl and Wei[12] of $Fe_2(CO)_6(\mu_2\text{-}SEt)_2$ fol-

Table I. Aromatic Parameters for $[Na(2,2,2\text{-crypt})]_2^+[Fe_2(CO)_6(\mu_2\text{-}PPh_2)_2]^{2-}$ [a,b]

A. Positional Parameters

	x	y	z		x	y	z
Fe	0.4726 (1)	0.8650 (1)	0.3352 (1)	HA(2)	0.5347	1.0781	0.3120
P	0.6089 (2)	1.0039 (2)	0.4611 (3)	HA(3)	0.6432	1.1322	0.1542
O(1)	0.3887 (6)	0.8543 (6)	0.0814 (8)	HA(4)	0.6833	0.9975	0.0818
C(1)	0.4229 (8)	0.8631 (7)	0.1854 (11)	HA(5)	0.8485	1.0077	0.0393
O(2)	0.3265 (6)	0.7274 (5)	0.3822 (8)	HA(6)	0.8235	0.9703	0.2912
C(2)	0.3877 (7)	0.7838 (6)	0.3664 (10)	HB(2)	0.3441	1.0811	0.4987
O(3)	0.6361 (6)	0.7358 (5)	0.1611 (8)	HB(3)	0.1310	1.0162	0.3008
C(3)	0.5704 (7)	0.7865 (7)	0.2315 (11)	HB(4)	0.1463	1.0092	0.2319
CA(1)	0.6756 (7)	1.0242 (6)	0.3188 (10)	HB(5)	0.0297	0.8625	0.2759
CA(2)	0.6132 (8)	1.0567 (7)	0.2628 (11)	HB(6)	0.1707	0.8610	0.4026
CA(3)	0.6514(11)	1.0650(7)	0.1434(12)	H(13A)	0.1472	0.5627	−0.0778
CA(4)	0.7577 (10)	1.0442 (8)	0.0817 (12)	H(13B)	0.2695	0.6868	0.0393
CA(5)	0.8180 (9)	1.0084 (8)	0.1387 (11)	H(14A)	0.0331	0.5875	0.9201
CA(6)	0.7746 (8)	0.9986 (7)	0.2531 (10)	H(14B)	0.1840	0.6759	1.0047
CB(1)	0.2716 (6)	1.0002 (6)	0.4568 (10)	H(16A)	0.3056	0.6582	0.7829
CB(2)	0.2779 (7)	1.0784 (7)	0.4406 (10)	H(16B)	0.2094	0.7420	0.8554
CB(3)	0.1947 (8)	1.0803 (8)	0.3681 (12)	H(17A)	0.2693	0.6963	0.6024
CB(4)	0.0960 (9)	0.9986 (10)	0.3096 (13)	H(17B)	0.1313	0.6318	0.5810
CB(5)	0.950 (8)	0.9236 (8)	0.3222 (14)	H(19A)	0.2694	0.5610	0.3255
CB(6)	0.1801 (8)	0.9241 (7)	0.3947 (12)	H(19B)	0.1414	0.4900	0.3225
Na	0.2264 (3)	0.4168 (3)	0.5548 (4)	H(20A)	0.3620	0.4184	0.2531
N(12)	0.2341 (6)	0.5189 (6)	0.9148 (8)	H(20B)	0.2660	0.3764	0.1080
C(13)	0.2074 (8)	0.6230 (7)	1.0116 (12)	H(22A)	0.1060	0.2380	0.0515
C(14)	0.1142 (8)	0.6273 (8)	0.9262 (12)	H(22B)	0.0680	0.3519	0.2131
O(15)	0.1436 (5)	0.5928 (4)	0.7701 (7)	H(23A)	0.0707	0.1656	0.1914
C(16)	0.2238 (8)	0.6646 (7)	0.7667 (12)	H(23B)	−0.0451	0.2070	0.1877
C(17)	0.2178 (8)	0.6379 (7)	0.6076 (11)	H(25A)	−0.0090	0.1714	0.4036
O(18)	0.2504 (5)	0.5418 (4)	0.4970 (7)	H(25B)	−0.1148	0.2442	0.4510
C(19)	0.2304 (9)	0.5030 (7)	0.3390 (12)	H(26A)	−0.0435	0.2820	0.6879
C(20)	0.2748 (8)	0.4058 (7)	0.2288 (11)	H(26B)	−0.0118	0.3885	0.6893
N(21)	0.2192 (6)	0.3275 (6)	0.2454 (8)	H(28A)	0.2291	0.3211	0.7830
C(22)	0.1072 (9)	0.2888 (8)	0.1818 (12)	H(28B)	0.0924	0.2887	0.8128
C(23)	0.0368 (8)	0.2327 (8)	0.2376 (12)	H(29A)	0.1666	0.4606	1.0413
O(24)	0.0374 (5)	0.2979 (5)	0.4025 (8)	H(29B)	0.0681	0.4677	0.9439
C(25)	−0.0263 (8)	0.2494 (8)	0.4658 (14)	H(30A)	0.3539	0.4465	0.9184
C(26)	0.0047 (8)	0.3130 (8)	0.6332 (13)	H(30B)	0.3600	0.5764	1.0850
O(27)	0.1169 (5)	0.3188 (5)	0.6499 (8)	H(31A)	0.5138	0.5637	0.9163
C(28)	0.1478 (8)	0.3403 (8)	0.7920 (14)	H(31B)	0.4224	0.6287	0.9146
C(29)	0.1513 (8)	0.4516 (8)	0.9335 (12)	H(33A)	0.3869	0.3403	0.6645
C(30)	0.3427 (8)	0.5217 (7)	0.9557 (11)	H(33B)	0.5275	0.4017	0.7095
C(31)	0.4311 (8)	0.5516 (7)	0.8764 (11)	H(34A)	0.5011	0.2606	0.4252
O(32)	0.4212 (5)	0.4810 (5)	0.7083 (7)	H(34B)	0.5337	0.3805	0.4589
C(33)	0.4528 (8)	0.3874 (8)	0.6477 (12)	H(36A)	0.4298	0.2022	0.1793
C(34)	0.4721 (8)	0.3320 (8)	0.4771 (12)	H(36B)	0.4419	0.3261	0.2319
O(35)	0.3723 (5)	0.3088 (5)	0.3990 (7)	H(37A)	0.2328	0.1745	0.1530
C(36)	0.3881 (9)	0.2673 (8)	0.2374 (12)	H(37B)	0.3413	0.2430	0.0817
C(37)	0.2788 (9)	0.2406 (7)	0.1602 (12)				

B. Anisotropic Temperature Factors ($\times 10^4$) [c,d]

	β_{11}	β_{22}	β_{33}	β_{12}	β_{13}	β_{23}		β_{11}	β_{22}	β_{33}	β_{12}	β_{13}	β_{23}
Fe	50	29	81	5	−2	30	O(15)	82	53	133	10	3	58
P	46	32	91	45	−16	35	C(16)	92	36	164	12	10	47
O(1)	130	95	145	3	−49	78	C(17)	90	43	145	12	0	56
C(1)	79	34	119	6	−4	30	O(18)	80	40	116	18	8	37
O(2)	115	48	177	5	26	63	C(19)	111	56	148	20	16	71
C(2)	54	30	126	2	−13	37	C(20)	97	58	108	11	27	58
O(3)	108	79	155	53	46	64	N(21)	77	44	100	3	−13	38
C(3)	55	40	127	5	−4	46	C(22)	110	73	136	2	−35	68
CA(1)	50	29	109	−1	−1	42	C(23)	84	66	149	−8	−25	50
CA(2)	78	56	110	6	6	51	O(24)	80	58	164	−4	−8	63
CA(3)	187	26	122	−5	−11	42	C(25)	69	72	270	−4	1	109
CA(4)	117	44	109	−25	39	9	C(26)	55	83	208	5	3	88
CA(5)	102	59	80	−21	8	18	O(27)	53	71	192	2	3	79
CA(6)	61	44	108	8	18	33	C(28)	66	95	287	6	−10	137
CB(1)	30	36	122	−4	−6	38	C(29)	82	68	150	−3	1	74
CB(2)	51	58	120	25	9	52	C(30)	54	70	132	5	−12	62
CB(3)	70	67	160	6	−37	46	C(31)	56	56	122	−3	−28	38
CB(4)	79	112	203	33	24	85	O(32)	64	58	131	25	20	54
CB(5)	57	72	266	−14	−48	85	C(33)	81	81	160	38	−18	49
CB(6)	59	55	209	−5	−23	75	C(34)	50	69	189	18	−18	44
Na	69	54	151	14	13	64	O(35)	51	67	133	19	9	54
N(12)	46	65	112	12	2	57	C(36)	86	75	115	32	38	49
C(13)	87	36	164	15	−7	35	C(37)	90	58	178	20	29	71
C(14)	53	96	170	10	4	94							

Table I (*Footnotes*)

[a] The estimated standard deviations of the least significant figures are given in parentheses. [b] The 2,2,2-crypt ligand denotes 4,7,13,16,21,24-hexaoxa-1,10-diazobicyclo[8.8.8]hexacosane, $N(C_2H_4OC_2H_4OC_2H_4)_3N$. [c] The anisotropic temperature factors are of the form $\exp[-(\beta_{11}h^2 + \beta_{22}k^2 + \beta_{33}l^2 + 2\beta_{12}hk + 2\beta_{13}hl + 2\beta_{23}kl)]$. These thermal coefficients were not varied in the final full-matrix least-squares cycle because of size limitations of the utilized configuration of the Harris SLASH 7 computer. [d] The isotropic temperature factor of each hydrogen atom was assigned a fixed value of 6.0 Å^2.

Table II. Interatomic Distances and Bond Angles for $[Na(2,2,2\text{-crypt})]_2^+[Fe_2(CO)_6(\mu_2\text{-}PPh_2)_2]^{2-}$

	A. Intraanion Distances (Å)[a]		
Fe···Fe′	3.630(3)	P-CA(1)	1.854(9)
		P-CB(1)	1.844(9)
Fe-P	2.271 (3)		
Fe-P′	2.288 (3)	CA(1)-CA(2)	1.40 (1)
		CA(2)-CA(3)	1.40 (1)
P···P′	2.759 (5)	CA(3)-CA(4)	1.43 (1)
		CA(4)-CA(5)	1.43 (1)
Fe-C(1)	1.771 (10)	CA(5)-CA(6)	1.38 (1)
Fe-C(2)	1.734 (9)	CA(6)-CA(1)	1.37 (1)
Fe-C(3)	1.746 (9)		
		CB(1)-CB(2)	1.42 (1)
C(1)-O(1)	1.155 (10)	CB(2)-CB(3)	1.38 (1)
C(2)-O(2)	1.179 (9)	CB(3)-CB(4)	1.49 (1)
C(3)-O(3)	1.158 (9)	CB(4)-CB(5)	1.35 (1)
		CB(5)-CB(6)	1.38 (1)
		CB(6)-CB(1)	1.38 (1)
	B. Selected Intraanion Nonbonding Distances (Å) between Carbonyl Atoms and Phenyl Carbon Atoms		
C(1)···CA(1)	3.46 (1)	C(2)···CA(2′)	3.17 (1)
O(1)···CA(2)	3.51 (1)	O(2)···CA(2′)	3.29 (1)
C(1)···CA(2)	3.30 (1)	C(2)···CB(1′)	3.72 (1)
C(1)···CB(1′)	3.13 (1)		
O(1)···CB(1′)	3.55 (1)	C(3)···CA(1)	3.48 (1)
C(1)···CB(6′)	3.51 (1)	C(3)···CA(6)	3.83 (1)
O(1)···CB(6′)	3.76 (1)	C(3)···CB(1)	3.42 (1)
		O(3)···CB(1)	3.80 (1)
C(2)···CA(1′)	3.10 (1)	C(3)···CB(2)	3.32 (1)
O(2)···CA(1′)	3.37 (1)	O(3)···CB(2)	3.53 (1)
	C. Intracation Bonding and Nonbonding Distances		
Na-N(12)	3.142 (8)	O(32)-C(33)	1.42 (1)
Na-O(15)	2.748 (7)	O(35)-C(34)	1.42 (1)
Na-O(18)	2.497 (7)	O(35)-C(36)	1.43 (1)
Na-N(21)	2.693 (8)		
Na-O(24)	2.664 (7)	O(15)···O(18)	2.784 (8)
Na-O(27)	2.554 (7)	O(24)···O(27)	2.737 (9)
Na-O(32)	2.715 (7)	O(32)···O(35)	2.781 (9)
Na-O(35)	2.532 (7)		
N(12)-C(13)	1.48 (1)	O(15)···N(12)	2.932 (9)
N(12)-C(29)	1.47 (1)	O(27)···N(12)	2.947 (10)
N(12)-C(30)	1.45 (1)	O(32)···N(12)	2.933 (9)
N(21)-C(20)	1.46 (1)	O(18)···N(21)	2.857 (9)
N(21)-C(22)	1.46 (1)	O(24)···N(21)	2.836 (10)
N(21)-C(37)	1.48 (1)	O(35)···N(21)	2.835 (9)
O(15)-C(14)	1.44 (1)	C(13)-C(14)	1.59 (1)
O(15)-C(16)	1.42 (1)	C(16)-C(17)	1.49 (1)
O(18)-C(17)	1.42 (1)	C(19)-C(20)	1.50 (1)
O(18)-C(19)	1.43 (1)	C(22)-C(23)	1.51 (1)
O(24)-C(23)	1.40 (1)	C(25)-C(26)	1.47 (1)
O(24)-C(25)	1.44 (1)	C(28)-C(29)	1.52 (1)
O(27)-C(26)	1.40 (1)	C(30)-C(31)	1.52 (1)
O(27)-C(28)	1.42 (1)	C(33)-C(34)	1.48 (1)
O(32)-C(31)	1.43 (1)	C(36)-C(37)	1.51 (1)
O(32)-C(33)	1.42 (1)		
	D. Closest Nonhydrogen Interionic Distances (Å)		
C(17)-CA(3)	4.00 (1)[b]	C(13)-C(1)	3.79 (1)[c]
O(35)-CB(3)	3.86 (1)[b]	C(13)-O(2)	3.58 (1)[c]
O(27)-CB(3)	3.51 (1)[b]	C(19)-O(2)	3.47 (1)
O(18)-O(2)	3.94 (1)	C(13)-C(2)	3.69 (1)[c]
C(13)-O(1)	3.74 (1)[c]		
	E. Intraanion Bond Angles (deg)		
		Fe-P′-CB(1′)	107.5 (3)
Fe-P-Fe′	105.5 (1)	CA(1)-P-CB(1)	101.0 (4)
P-Fe-P′	74.5 (1)	P-CA(1)-CA(2)	116.3 (7)
		P-CA(1)-CA(6)	124.6 (7)

Table II (*Continued*)

P-Fe-C(1)	104.9 (3)		
P-Fe-C(2)	139.5 (3)	CA(1)-CA(2)-CA(3)	121.1 (9)
P-Fe-C(3)	89.7 (3)	CA(2)-CA(3)-CA(4)	120.0 (10)
P′-Fe-C(1)	96.4 (3)	CA(3)-CA(4)-CA(5)	117.2 (10)
P′-Fe-C(2)	88.6 (3)	CA(4)-CA(5)-CA(6)	120.1 (10)
P′-Fe-C(3)	159.8 (3)	CA(5)-CA(6)-CA(1)	122.7 (9)
		CA(6)-CA(1)-CA(2)	118.6 (8)
Fe-C(1)-O(1)	175.1 (8)	P-CB(1)-CB(2)	119.1 (6)
Fe-C(2)-O(2)	176.7 (8)	P-CB(1)-CB(6)	124.2 (3)
Fe-C(3)-O(3)	178.3 (8)		
		CB(1)-CB(2)-CB(3)	121.6 (9)
C(1)-Fe-C(2)	113.5 (4)	CB(2)-CB(3)-CB(4)	117.9 (10)
C(1)-Fe-C(3)	99.9 (4)	CB(3)-CB(4)-CB(5)	118.4 (10)
C(2)-Fe-C(3)	95.7 (4)	CB(4)-CB(5)-CB(6)	121.8 (10)
		CB(5)-CB(6)-CB(1)	122.2 (9)
Fe-P-CA(1)	109.1 (3)	CB(6)-CB(1)-CB(2)	117.9 (8)
Fe-P-CB(1)	119.1 (3)		
Fe-P′-CA(1′)	115.0 (3)		

F. Bond Angles (deg) within the $[Na(2,2,2\text{-crypt})]^+$ Cation

N(12)-Na-O(15)	59.3 (2)	N(12)-C(13)-C(14)	110.5 (8)
N(12)-Na-O(27)	61.3 (2)	C(13)-C(14)-O(15)	111.9 (8)
N(12)-Na-O(32)	59.6 (2)	C(14)-O(15)-C(16)	113.6 (8)
O(15)-Na-O(18)	63.9 (2)	O(15)-C(16)-C(17)	107.7 (8)
O(18)-Na-N(21)	66.7 (2)	C(16)-C(17)-O(18)	108.1 (7)
N(21)-Na-O(24)	63.9 (2)	C(17)-O(18)-C(19)	111.6 (7)
N(21)-Na-O(35)	65.6 (2)	O(18)-C(19)-C(20)	108.8 (7)
O(24)-Na-O(27)	63.2 (2)	C(19)-C(20)-N(21)	111.2 (8)
O(32)-Na-O(35)	63.9 (2)		
		N(21)-C(22)-C(23)	112.9 (8)
O(15)-Na-O(35)	156.8 (2)	C(22)-C(23)-O(24)	109.0 (8)
O(18)-Na-O(27)	153.0 (2)	C(23)-O(24)-C(25)	112.6 (8)
O(24)-Na-O(32)	159.7 (2)	O(24)-C(25)-C(26)	107.2 (8)
		C(25)-C(26)-O(27)	109.8 (8)
N(12)-Na-N(21)	179.4 (2)	C(26)-O(27)-C(28)	114.8 (8)
		O(27)-C(28)-C(29)	113.1 (8)
N(12)-Na-O(18)	113.9 (2)	C(28)-C(29)-N(12)	110.7 (8)
N(12)-Na-O(24)	115.7 (2)		
N(12)-Na-O(35)	114.2 (2)	N(12)-C(30)-C(31)	111.4 (7)
N(21)-Na-O(15)	121.2 (2)	C(30)-C(31)-O(32)	112.7 (8)
N(21)-Na-O(27)	118.2 (2)	C(31)-O(32)-C(33)	112.3 (7)
N(21)-Na-O(32)	120.6 (2)	O(32)-C(33)-C(34)	108.7 (9)
		C(33)-C(34)-O(35)	109.0 (8)
O(15)-Na-O(24)	96.7 (2)	C(34)-O(35)-C(36)	111.9 (7)
O(15)-Na-O(27)	94.7 (2)	O(35)-C(36)-C(37)	109.1 (8)
O(15)-Na-O(32)	96.6 (2)	C(36)-C(37)-N(21)	112.8 (8)
O(18)-Na-O(24)	101.3 (2)		
O(18)-Na-O(32)	98.3 (2)	C(13)-N(12)-C(29)	110.2 (7)
O(18)-Na-O(35)	104.8 (2)	C(13)-N(12)-C(30)	110.9 (7)
O(24)-Na-O(35)	105.6 (2)	C(29)-N(12)-C(30)	110.8 (7)
O(27)-Na-O(32)	100.4 (2)	C(20)-N(21)-C(22)	111.2 (8)
O(27)-Na-O(35)	100.8 (2)	C(20)-N(21)-C(37)	110.0 (8)
		C(22)-N(21)-C(37)	108.3 (8)

G. Dihedral Angles (deg) within the $[Na(2,2,2\text{-crypt})]^+$ Cation

N(12)-C(13)-C(14)-O(15)	113.0	C(25)-C(26)-O(27)-C(28)	−175.5
C(13)-C(14)-O(15)-C(16)	108.0	C(26)-O(27)-C(28)-C(29)	114.4
C(14)-O(15)-C(16)-C(17)	160.2	N(12)-C(29)-C(28)-O(27)	−117.4
O(15)-C(16)-C(17)-O(18)	114.1	N(12)-C(30)-C(31)-O(32)	−119.2
C(16)-C(17)-O(18)-C(19)	170.7	C(30)-C(31)-O(32)-C(33)	−107.0
C(17)-O(18)-C(19)-C(20)	175.5	C(31)-O(32)-C(33)-C(34)	163.4
O(18)-C(19)-C(20)-N(21)	−117.9	O(32)-C(33)-C(34)-O(35)	−107.3
O(24)-C(23)-C(22)-N(21)	123.2	C(33)-C(34)-O(35)-C(36)	−172.4
C(22)-C(23)-O(24)-C(25)	−178.9	C(34)-O(35)-C(36)-C(37)	−177.8
C(23)-O(24)-C(25)-C(26)	164.6	O(35)-C(36)-C(37)-N(21)	126.3
O(24)-C(25)-C(26)-O(27)			

[a] Primed atoms (e.g., Fe′) refer to the symmetry-related position $1-x, 2-y, 1-z$. [b] Related by $x, -1+y, z$. [c] Related by $x, y, -1+z$.

lowed shortly by an X-ray diffraction analysis by them[13] in 1965 of the $Fe_2(CO)_6(\mu_2\text{-}S_2)$ molecule. The latter study revealed a bridging disulfide ligand coordinated sideways to the two iron atoms and hence furnished the first example that the Fe_2E_2 cores may possess direct E–E bonds in addition to Fe–Fe bonds. The similarly shaped, highly bent Fe_2S_2 cores in these two dimers with essentially identical acute Fe–S–Fe bond angles of 68 vs. 70° and short Fe–Fe distances of 2.54 vs. 2.55

Table III. Least-Squares Planes for the $[Fe_2(CO)_6(\mu_2\text{-}PPh_2)_2]^{2-}$ Dianion

A. Equations Defining Least-Squares Planes[b]

plane I, through Fe, Fe', P, P'
$-0.3302X + 0.7369Y - 0.5899Z - 6.1362 = 0$
plane II, through P, C(1), C(2)
$0.7290X - 0.3518Y - 0.5872Z + 3.6905 = 0$
plane III, through P', Fe, C(3)
$0.2416X + 0.9310Y - 0.2737Z - 11.2575 = 0$
plane IV, through P, P', C(3)
$-0.3327X + 0.6440Y - 0.6889Z - 4.4777 = 0$
plane V, through P, P', C(2), C(3)
$-0.4461X + 0.5126Y - 0.7336Z - 2.1700 = 0$
plane VI, through Fe, P, C(1)
$0.7437X - 0.2314Y - 0.6272Z + 2.1479 = 0$
plane VII, through Fe, P', C(1)
$-0.6719X - 0.7289Y - 0.1312Z + 11.3824 = 0$

B. Perpendicular Distances (Å) of Some Atoms from Designated Planes

	I	II	III	IV	V	VI	VII
Fe	0	0.15	0	0.24	0.46	0	0
Fe'	0	−2.22	1.40	−0.24	−0.46	−2.20	−2.12
P	0	0	1.40	0	−0.17	0	−2.12
P'	0	−2.06	0	0	0.17	−2.20	0
C(1)	1.71	0	1.04	2.00	2.24	0	0
C(2)	−1.05	0	−1.69	−0.68	−0.19	−0.36	1.59
C(3)	−0.39	1.89	0	0	0.19	1.72	−0.36

C. Angles (deg) between Normals to the Designated Planes

	I	II	III	IV	V	VI	VII
I		98.8	39.8	7.8	16.7	92.6	103.8
II			89.5	93.7	94.3	7.3	99.0
III				44.9	55.2	82.2	143.6
IV					10.3	88.0	98.9
V						89.4	88.7
VI							104.4

[a] Atoms with primes (e.g., P') refer to the symmetry-related position $1-x, 2-y, 1-z$. [b] The equations of the planes are given in an orthogonal ångstrom coordinate system (X, Y, Z) which is related to the fractional unit cell coordinate system (x, y, z) as follows: $X = xa + yb\cos\gamma + zc\cos\beta$; $Y = yb\sin\gamma + zc\cos\mu$; $Z = zc\cos\sigma$. Here $\cos\mu = (\cos\alpha - \cos\beta\cos\gamma)/\sin\gamma$ and $\sin^2\sigma = 1 - \cos^2\beta - \cos^2\mu$; all atoms were assigned unit weights.

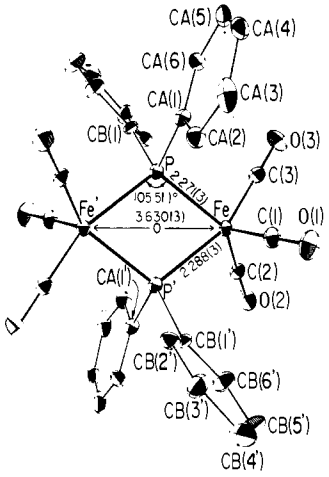

Figure 2. Configuration of the $[Fe_2(CO)_6(\mu_2\text{-}PPh_2)_2]^{2-}$ dianion of the $[Na(2.2.2\text{-crypt})]^+$ salt. The dianion conforms exactly to crystallographic C_i-$\bar{1}$ site symmetry.

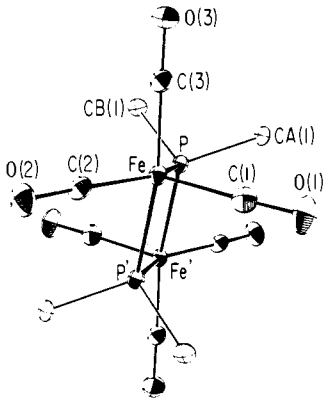

Figure 3. View of $[Fe_2(CO)_6(\mu_2\text{-}PPh_2)_2]^{2-}$ dianion (with phenyl rings omitted for clarity) emphasizing the considerable observed distortions of the carbonyl ligands from an idealized C_{2h}-$2/m$ geometry arising from a formal construction of the dimer by the junction of two trigonal bipyramids along an equatorial–axial edge.

Å were attributed[13] to the formation of a distinct "bent" electron-pair Fe–Fe bond. Since then, the size of the $Fe_2(CO)_6X_2$ class has grown immensely, and X-ray diffraction studies[7,14-16] have been performed on a large variety of nitrogen-, phosphorus-, sulfur-, and arsenic-bridged diiron hexacarbonyl dimers including several PRR'-bridged species (with R = R' = Ph, Me; R = Ph, R' = Me, H; R = Me, R' = H).[6] An important observed structural feature in these homologous complexes (Figure 1) is the general occurrence (in the absence of abnormal steric effects) of a symmetrical Fe_2E_2-bridged fragment of idealized C_{2v} geometry with analogous Fe–Fe distances and resembling Fe–E–Fe bond angles for similar X ligands. Geometrical variations among the Fe_2E_2 cores in these dimers have also been described in terms of the torsional angle[14] θ (denoted elsewhere[17] as a dihedral or hinge angle) between the two planes each formed by the two bridging E atoms and one M atom.

In order to assess the degree of responsibility of the Fe–Fe bonds on the resembling molecular geometries of these dimers, syntheses of the presumably corresponding $Co_2(CO)_6(SR)_2$ dimers (R = Et, Ph), reported by Hieber and Spacu[18] in 1937 but never confirmed, and the presumed red $Co_2(CO)_6(PPh_2)_2$ dimer, first reported in a patent by Schweckendieck[19] in 1959 and later by Hayter[20] in 1963, were attempted in our laboratories, first ca. 1966 and then later. These cobalt complexes, which were presumed from electronic considerations to differ from the iron dimers in not having metal–metal interactions (i.e., not required in order for each metal to achieve a closed-shell electronic configuration), would also have possessed an

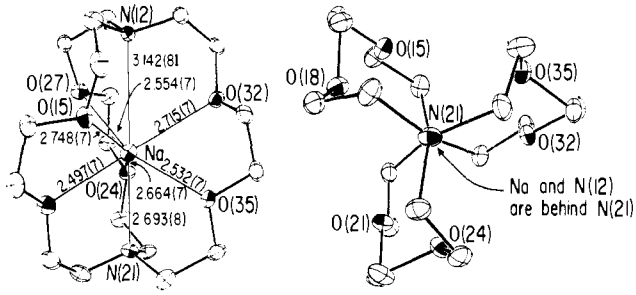

Figure 4. Two views of the $[Na(2,2,2\text{-crypt})]^+$ cation of the $[Fe_2(CO)_6(\mu_2\text{-}PPh_2)_2]^{2-}$ salt, showing (a) the asymmetrical coordination of the encapsulated Na^+ cation and (b) the approximate D_3 symmetry of the cryptate ligand viewed down the N(21)-Na-N(12) axis. The 2,2,2-crypt denotes $N(C_2H_4OC_2H_4OC_2H_4)_3N$.

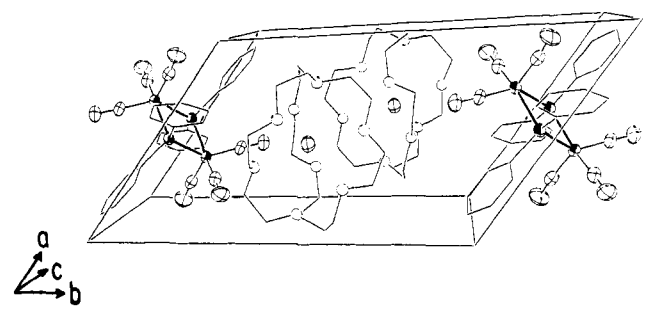

Figure 5. View of the triclinic unit cell of $[Na(2,2,2\text{-crypt})]_2^+[Fe_2(CO)_6(\mu_2\text{-}PPh_2)_2]^{2-}$ showing the arrangement under $P\bar{1}$ symmetry of the two monocations of general site symmetry C_1-1 and the one dianion of special site symmetry C_i-$\bar{1}$.

unprecedented (and at that time unknown) type of ligand-bridged dimeric geometry (in the absence of direct metal-metal bonding) with three terminal monodentate and two bridging atoms coordinated to each five-coordinate metal atom. Our attempted preparations of the ethylmercaptocobalt and phenylmercaptocobalt carbonyl dimers instead resulted in the synthesis and structural characterization of $Co_5(CO)_{10}(SEt)_5$[21] and $Co_3(CO)_9(\mu_3\text{-}S)$,[22] respectively, both of which possess unusual structural and bonding features. Our preparation and isolation of the presumed $Co_2(CO)_6(PPh_2)_2$ dimer by the Hayter procedure[20,23] invariably yielded red powder, from which repeated efforts to obtain crystals for X-ray diffraction were unsuccessful. On the basis of Hayter's molecular-weight measurements[20] of this compound in benzene either by osmometry or by boiling-point elevation giving unexpectedly high values (in the 6000–8000 g/mol range), our current belief is that this presumed dimer is instead a polymeric species.[24]

The first experimental evidence that the molecular geometry of the electron spin-coupling interaction in a neutral $Fe_2(CO)_6X_2$-type dimer was strongly dependent on the Fe–Fe interaction was provided by structural determinations[25] in 1967 of the two diphenylphosphido-bridged $M_2(\eta^5\text{-}C_5H_5)_2(\mu_2\text{-}PPh_2)_2$ dimers (where M = Co, Ni) which were initially prepared and spectroscopically characterized by Hayter.[26] These molecular complexes differ from each other only by the necessity of an electron-pair interaction in the cobalt dimer as opposed to none in the nickel dimer in order for the metal atoms to achieve a closed-shell electronic configuration in conformity with the diamagnetism of both compounds. A separate M–M single bond of strength equivalent to that found in dimeric organometallic complexes linked only by metal–metal bonds was proposed[25] in the cobalt dimer to account for (1) the marked decrease of 0.80 Å in the metal–metal distance from a nonbonding value of 3.36 Å in the nickel dimer to a bonding value of 2.56 Å in the cobalt dimer and (2) the concomitant bending deformation of the M_2P_2 framework from a planar Ni_2P_2 core in the nickel dimer (with $\theta = 180°$) to a highly nonplanar Co_2P_2 core (with $\theta = 105°$) resulting in a decrease of the bridging M–P–M′ angle by 30° from a relatively unstrained value of 102.4° in the nickel dimer to a sharply acute value of 72.5° in the cobalt dimer. The close similarity of the molecular configurations of the electronically equivalent $Fe_2(CO)_6(\mu_2\text{-}SEt)_2$ and $Co_2(\eta^5\text{-}C_5H_5)_2(\mu_2\text{-}PPh_2)_2$ dimers (in which each cyclopentadienyl ring occupies the three coordination sites of three carbonyl ligands) was cited[25] as evidence that the bond strengths of the electron-pair Fe–Fe interactions in the $Fe_2(CO)_6X_2$ dimers are likewise *not* characteristic of weak spin-pairing interactions.

In 1968 Dessy et al.[27] reported that $Fe_2(CO)_6(\mu_2\text{-}PMe_2)_2$ undergoes an electrochemically reversible two-electron reduction to the $[Fe_2(CO)_6(\mu_2\text{-}PMe_2)_2]^{2-}$ dianion, which is electronically equivalent to the previously sought after $Co_2(CO)_6(\mu_2\text{-}X)_2$ dimers (X = SR, PR_2). They also generated an equilibrium mixture containing the radical monoanion by reaction of the diamagnetic dianion, which displays no ESR signal, with the neutral parent. Based on an electrochemical isolation of the dianion by exhaustive controlled-potential electrolysis, Dessy and Wieczorek[28] in 1969 published an infrared spectral analysis of the neutral dimer and dianion. In 1972 Dessy, Rheingold, and Howard[29a] presented the results of a detailed ^1H NMR, ESR, and Mössbauer study for the entire $[Fe_2(CO)_6(\mu_2\text{-}PMe_2)_2]^n$ series ($n = 0, -1, -2$). They concluded from their spectroscopic solution measurements, which showed that the exo and endo methyl hydrogen substituents are not equivalent in the two anions ($n = -1, -2$), that the dimethylphosphido-bridged dimer maintains its nonplanarity in both the monoanion and dianion. They found that the neutral parent and dianion both exhibit similar variable-temperature ^1H NMR spectra which they interpreted in terms of analogous fluxional behavior with methyl exchange occurring via an intramolecular inversion pathway not involving bond cleavage. At the same time they also suggested from an analysis of their data that the M–M bond is retained in the dianion and that the two additional electrons in the dianion primarily strengthen the Fe–P bonds. Shortly thereafter, Dessy and Bares[29b] reinterpreted the spectroscopic data in accord with the premise (previously advocated by us[25,30,31] from structural studies of ligand-bridged dimers with and without metal–metal bonds) that the additional two electrons in the dianion instead occupy a MO comprised mainly of antibonding dimetal orbital character.

This comprehensive work of Dessy et al.[27-29] prompted Teo et al.[7] to include the $[Fe_2(CO)_6(\mu_2\text{-}PPh_2)_2]^n$ series ($n = 0, -1, -2$) in a systematic theoretical investigation via the nonparametrized Fenske–Hall MO model of representative $Fe_2(CO)_6X_2$ dimers with and without E–E bonds. These comparative calculations[7] yielded MO wave functions and energy-level orderings consistent with (1) the HOMO in each neutral species corresponding to the classical "bent" Fe–Fe bond, and (2) the LUMO being of predominantly antibonding diiron character, occupied by one electron in the monoanion and by two electrons in the dianion, corresponding formally to a "net" one-electron and a "net" no-electron Fe–Fe bond, respectively.

The influence of the Fe–P as well as Fe–Fe interactions in changing the torsional angle θ (and simultaneously the Fe–Fe distance) of the Fe_2P_2 core in neutral $Fe_2(CO)_6(\mu_2\text{-}PR_2)_2$ dimers upon variation of R substituents with markedly different electronegativities was later investigated by Burdett[17] from extended Hückel MO calculations based in large part on the molecular parameters recently determined by Clegg[15] for the neutral $Fe_2(CO)_6(\mu_2\text{-}P(CF_3)_2)_2$ dimer. Upon formal replacement of phosphorus-attached H, Me, or Ph substituents

with highly electronegative CF_3 substituents, Burdett[17] attributed the unexpectedly large increase of 0.2 Å in the electron-pair Fe–Fe distance (from values of range 2.623 (2) to 2.665 (2) Å with θ varying from 100 to 107° to a value of 2.819 (1) Å with $\theta = 119°$) to the HOMO being Fe–P antibonding as well as Fe–Fe bonding. He also pointed out that electron occupation of the LUMO of the neutral dimer upon reduction to the dianion should strongly favor a geometrical change from a bent to planar Fe_2P_2 core (with $\theta = 180°$) on account of reduced Fe–P repulsion as well as reduced Fe–Fe repulsion.

B. Its Overall Structure and Properties. The configuration of the $[Fe_2(CO)_6(\mu_2\text{-}PPh_2)_2]^{2-}$ dianion (Figure 2), which unequivocally contains no Fe–Fe bond (vide infra), is best described as formally arising from two distorted trigonal bipyramids which share a common axial–equatorial edge. The Fe_2P_2 core is strictly planar, as required by a crystallographic inversion center in the middle of the dimer. Hence, each of the two equivalent phosphorus atoms is axial to one iron atom and equatorial to the other iron atom. Figure 3 shows for a trigonal-bipyramidal coordination at each zerovalent iron that the carbonyl C(3) atom is axial and the carbonyl C(1) and C(2) atoms are equatorial. This view of the dimer also reveals considerable distortions of the $Fe_2(CO)_6P_2$ fragment from an idealized C_{2h}-$2/m$ geometry formed from two edge-shared trigonal bipyramids. Nevertheless, an examination of the particular deformations (vide infra) makes it more appropriate to utilize a trigonal-bipyramidal rather than a tetragonal-pyramidal description for the five-coordinate iron atoms. This dianion is one of only a few crystallographic examples[32-34] of a (metal–metal)-nonbonded dimer formed by an edge sharing of two trigonal bipyramids (vide infra).

A cyclic voltammogram of the neutral $Fe_2(CO)_6(\mu_2\text{-}PPh_2)$ parent, obtained at a mercury electrode in acetonitrile with 0.2 M $(NEt_4)ClO_4$ as supporting electrolyte, exhibits a single two-electron, reversible reduction wave.[2] This reduction in a single two-electron step appears to be distinctly different from the reduction reported by Dessy et al.[27,29a] for the neutral dimethylphosphido-bridged analogue in 1,2-dimethoxyethane. Although it was stated by Dessy, Rheingold, and Howard[29a] that the dimethylphosphido-bridged diiron complex exhibits one two-electron, polarographic reduction wave which is unsplit upon investigation by cyclic voltammetry, their ESR evidence from solution mixtures of the diamagnetic neutral parent and corresponding diamagnetic dianion for the presence of the paramagnetic $[Fe_2(CO)_6(\mu_2\text{-}PMe_2)_2]^-$ monoanion points to the following conclusions: (1) $Fe_2(CO)_6(\mu_2\text{-}PMe_2)_2$ reduces in two one-electron steps; (2) the reduction potential for the introduction of the second electron is equal to or falls more cathodic than that of the first electron. In contrast, for the $Fe_2(CO)_6(\mu_2\text{-}PPh_2)_2$ dimer there was no detection by ESR spectroscopy of any paramagnetic species upon a mixing of equal volumes of 10^{-3} M solutions of $Fe_2(CO)_6(\mu_2\text{-}PPh_2)_2$ and $Na_2^+[Fe_2(CO)_6(\mu_2\text{-}PPh_2)_2]^{2-}\cdot 5THF$, both of which are diamagnetic, in 2-methyltetrahydrofuran.[2b] Additional attempts[2b] to detect the hypothetical $[Fe_2(CO)_6(\mu_2\text{-}PPh_2)_2]^-$ monoanion by examination of the infrared and visible spectra of a mixture of equal volumes of 10^{-1} M solutions of the neutral dimer and the dianion in tetrahydrofuran were also unsuccessful. Hence, the lack of any evidence for an intermediate monoanion is in accordance with the cyclic voltammetric measurements indicating that the reduction takes place in a single two-electron step. It was thereby concluded[2b] in this case that the reduction potential for the introduction of the second electron falls more anodic than that of the first electron. The results of this structural study indicate that intramolecular steric effects may be invoked to rationalize these different redox properties between the diphenylphosphido- and dimethylphosphido-bridged dimers. It is noteworthy that the determined $E_{1/2}$ value of −1.26 V (vs. the aqueous SCE with 0.2 M $(Et_4N)ClO_4$ as supporting electrolyte)[2] for the diphenylphosphido-bridged dimer is comparable to the value for the dimethylphosphido-bridged dimer of −2.1 V (vs. the $AgClO_4|Ag$ electrode with 0.1 M $(Bu_4N)ClO_4$ as supporting electrolyte),[27,29a] which on the basis of an estimated potential difference of +0.7 V between the two reference electrodes[35] corresponds to a value of −1.4 V (vs. the aqueous SCE).

The carbonyl stretching frequencies obtained from an infrared spectrum of $Na_2[Fe_2(CO)_6(\mu_2\text{-}PPh_2)_2]\cdot 5THF$ as a THF solution display an overall intensity pattern analogous to that in the carbonyl stretching region obtained by Dessy and Wieczorek[28] from an infrared spectrum of the $[Fe_2(CO)_6(\mu_2\text{-}PMe_2)_2]^{2-}$ dianion (prepared by exhaustive controlled-potential electrolysis) in 1,2-dimethoxyethane solution (also containing 0.1 M TBAP). A comparison between the diphenylphosphido- and dimethylphosphido-bridged compounds of the corresponding carbonyl frequencies (viz., 1930 (m) vs. 1909 (w), 1905 (vs) vs. 1879 (vs), 1845 (vs) vs. 1810 (vs), and 1825 (s) and 1800 (vs) vs. 1800 (vs) cm^{-1}) reflects an expected carbonyl frequency shift associated with the greater inductive effect of the alkyl substituents.

Group theoretical considerations based on C_{2h} symmetry for the $Fe_2(CO)_6P_2$ part of the $[Fe_2(CO)_6(\mu_2\text{-}PPh_2)_2]^{2-}$ dianion lead to the prediction of six vibrational C–O stretching modes ($2A_g + B_g + A_u + 2B_u$), of which three ($A_u + 2B_u$) are IR active and three ($2A_g + B_g$) are Raman active. The lack of high-resolution spectral data coupled with the considerable deviation of the $Fe_2(CO)_6$-P_2 fragment of the $[Fe_2(CO)_6(\mu_2\text{-}PPh_2)_2]^{2-}$ dianion in the solid state from an idealized C_{2h} geometry preclude a tentative assignment of the carbonyl bands.

C. The Fe_2P_2 Core and Its Stereochemical Relationship with the Fe_2P_2 Core of the Neutral Parent. An examination of the observed changes in the geometry of the central Fe_2P_2 core of the $Fe_2(CO)_6(\mu_2\text{-}PPh_2)_2$ dimer (Figure 1) upon reduction to the dianion (Figures 2 and 3) provides a direct experimental probe of the topological nature of the LUMO in the neutral parent, to which two electrons are added in the dianion. The considerable antibonding bimetallic character of this resulting HOMO in the dianion is reflected by the large increase of the Fe–Fe distance by 1.01 Å from an electron-pair bonding value of 2.623 (2) Å to a nonbonding value of 3.630 (3) Å in the dianion.

The other noteworthy bond-length change observed upon reduction of the neutral dimer to the dianion is a small but significant lengthening of 0.05 Å in the Fe–P bonds. In the dianion the bond length of 2.288 (3) Å from the independent Fe atom to its axial P′ atom (shown in Figure 3) is only 0.017 Å longer than that of 2.271 (3) Å from the Fe atom to its equatorial P atom. However, the mean of 2.280 Å in the dianion is distinctly longer than the mean of 2.233 Å (from four independent Fe–P values of range 2.228 (3)–2.240 (3) Å in $Fe_2(CO)_6(\mu_2\text{-}PPh_2)_2$). Although part of the longer Fe–P bond lengths in the dianion may be ascribed to steric effects due to crowding of the phenyl rings[36] (vide infra), the crystallographic data indicate that the LUMO in the neutral parent also has significant Fe–P antibonding character.

The striking geometrical consequence of the two-electron population of the LUMO is a diminishing of both Fe–Fe and Fe–P repulsions by a complete flattening of the highly bent Fe_2P_2 core along the P···P line from a torsional θ angle of only 100° in the neutral dimer to $\theta = 180°$ in the dianion. This degree of angular distortion also produces a dramatic increase of 33.5° in the bridging Fe–P–Fe′ angle from a highly acute angle of 72.0° in the neutral dimer to a relatively unstrained tetrahedral angle of 105.5° in the dianion.

The observed decrease in the P···P distance from 2.866 (3) to 2.759 (5) Å upon reduction of $Fe_2(CO)_6(\mu_2\text{-}PPh_2)_2$ to its dianion is consistent with the previous ^1H NMR study by

Table IV. Comparison of the Observed Coordination Angles (deg) about Each Five-Coordinate Iron in the $[Fe_2(CO)_6(\mu_2\text{-}PPh_2)_2]^{2-}$ Dianion with Idealized Values for Regular Trigonal-Bipyramidal and Tetragonal-Pyramidal Geometries

bond angles	actual	TBP[a]	SP[a]
C(3)-Fe-P	89.7(3)	90	90 (<90)
C(3)-Fe-C(1)	99.9(4)	90	90 (>90)
C(3)-Fe-C(2)	95.7(4)	90	90 (<90)
P′-Fe-P	74.5(1)	90	90 (<90)
P′-Fe-C(1)	96.4(3)	90	90 (>90)
P′-Fe-C(2)	88.6(3)	90	90 (<90)
P-Fe-C(2)	139.5(3)	120	180 (<180)
C(1)-Fe-C(2)	113.5(4)	120	90 (>90)
C(1)-Fe-P	104.9(3)	120	90 (>90)
P′-Fe-C(3)	159.8(3)	180	180 (<180)

[a] For an assumed trigonal-bipyramidal coordination (TBP), the axial ligands are C(3) and P′ with C(1), C(2), and P being equatorial; for an assumed square-pyramidal coordination (SP), C(1) is designated as the axial ligand and C(2), C(3), P, and P′ as the basal ligands. For an idealized SP configuration, the nonparenthesized angles are based upon each equivalent iron atom being situated in the basal plane, while the corresponding parenthesized angles are based upon each iron atom being displaced out of the basal plane toward the axial C(1) ligand.

Dessy and co-workers,[29] who found for the corresponding $[Fe_2(CO)_6(\mu_2\text{-}PMe_2)_2]^n$ dimers ($n = 0, -2$) a large increase in the nuclear coupling between the phosphorus atoms from 85 ± 10 Hz for $n = 0$ to >500 Hz for $n = -2$. The MO calculations by Teo et al.[7] pointed to the existence of net attractive P···P bonding interactions in the model $[Fe_2(CO)_6(\mu_2\text{-}PH_2)_2]^n$ series ($n = 0, -1, -2$).

D. Disposition of the Carbonyl Ligands and Relationship of the Five-Coordinate Metal Atoms with Those in the $[Cu_2Cl_6(\mu_2\text{-}Cl)_2]^{4-}$ and $[Ni_2Cl_6(\mu_2\text{-}Cl)_2]^{4-}$ Dimers. Although the architecture of the dianion can best be described as two trigonal bipyramids sharing a common axial-equatorial edge (Figure 3), there are significant distortions by which the C_{2h}-$2/m$ symmetry for the idealized geometry of the $Fe_2(CO)_6P_2$ fragment is reduced to the crystallographically required C_i-$\bar{1}$ symmetry.

Under assumed trigonal-bipyramidal symmetry for the crystallographically independent Fe atom, the C(3) and P′ atoms form the axial ligand atoms and the P, C(1), and C(2) atoms the equatorial ligand atoms. The iron and three equatorial ligand atoms are nearly coplanar with the Fe atom perpendicularly displaced by only 0.15 Å out of the equatorial ligand-atom plane toward C(3). The axial C(3)–O(3) ligand, which is perpendicular within 0.3° to the equatorial Fe–P bond, is tipped somewhat out of the Fe_2P_2 plane, as indicated by C(3) being displaced by 0.39 Å from the Fe_2P_2 plane and by a dihedral angle of 39.8° between the normals of the C(3)–Fe–P and Fe_2P_2 planes instead of 0° for a regular trigonal bipyramid. Figure 3 shows that the observed large distortions from this idealized geometry are primarily associated with the equatorial C(1)–O(1) and C(2)–O(2) ligands, which under C_{2h}-$2/m$ symmetry are related to each other by the horizontal mirror plane coincident with the planar Fe_2P_2 core. These two equatorial carbonyl ligands, for which the C(1)–Fe–C(2) angle of 113.5 (4)° is reasonably close to the idealized value of 120°, are displaced from mirror-plane symmetry mainly by a rotation about the Fe–P'_{ax} line toward the equatorial phosphorus atom, P_{eq}. The resulting P_{eq}–Fe–C(1) and P_{eq}–Fe–C(2) angles of 104.9 (3) and 139.5 (3)°, respectively, are smaller and greater, respectively, than an idealized value of 120°. The small deformation of these two carbonyl ligands out of the equatorial plane is indicated by the P'_{ax}–Fe–C(1) and P'_{ax}–Fe–C(2) angles of 96.4 (3) and 88.6 (3)°, respectively, being nearer the idealized value of 90°.

These carbonyl displacements can be readily ascribed to intraanionic steric overcrowding primarily involving repulsions between the carbonyl ligands and the phenyl substituents of the phosphorus atoms. Table II gives the closest nonbonding contacts between the three carbonyl ligands and phenyl rings. The shortest observed separations of 3.10 Å between the C(2) atom and the phosphorus-attached CA(1′) atom and of 3.13 Å between the C(1) atom and the phosphorus-linked CB(1′) atom provide a rationalization for the occurrence of the above-mentioned rotational-like distortion of the C(1)–O(1) and C(2)–O(2) ligands about the Fe–P'_{ax} line in that any backward rotation would produce a further shortening of these two distances.

Evidence that the coordination about each iron atom is more readily envisioned as a distorted trigonal bipyramid than as a distorted tetragonal pyramid is found in Table IV, which lists the relevant bond angles found in the dianion and compares them to those for regular trigonal-bipyramidal and tetragonal-pyramidal configurations.

A rearrangement of the carbonyl ligands must occur upon reduction of the neutral dimer (Figure 1) to its dianion (Figures 2 and 3). As the highly bent Fe_2P_2 core in the neutral dimer flattens in the dianion in order to reduce both Fe–Fe and Fe–P repulsions, a rotation of the carbonyls about at least one of the resulting five-coordinate iron atoms is necessary in order to interconvert the $Fe_2(CO)_6P_2$ part of the dimer from the idealized C_{2v} geometry of the neutral parent to the idealized centrosymmetric C_{2h} geometry of the dianion. A rationale for such a pseudorotation of carbonyl ligands can be readily found in the fluxionality of trigonal-bipyramidal phosphorus molecules where several mechanisms, such as the widely accepted Berry pseudorotation mechanism,[37] are well known. This mechanism is particularly appealing in that it requires a square-pyramidal intermediate (analogous to the square-pyramidal environment of carbonyl and phosphorus ligands about each iron atom in the neutral $Fe_2(CO)_6(\mu_2\text{-}PPh_2)_2$ dimer) for site exchange of the equatorial and axial ligands in a trigonal-bipyramidal molecule. In fact, Adams and Cotton[38] in their ^1H NMR investigation of the stereochemical nonrigidity of the (Co-Co)-bonded $Co_2(CO)_6(\mu_2\text{-}GeMe_2)_2$ analogue of the neutral phosphido-bridge iron dimer explicitly pointed out that their proposed methyl site-exchange pathway (involving a transition state or intermediate with a trigonal-bipyramidal ligand configuration about each cobalt atom) represents the converse of the Berry mechanism. A recent comprehensive examination by Cotton, Cullen, and their coworkers[39] of the fluxional behavior of a number of compounds of the (metal–metal)-bonded $M_2(CO)_6(\mu_2\text{-}X)_2$-type dimer (with X = PMe_2, $AsMe_2$, AsMePh, SMe, and SEt for M = Fe and X = $GeMe_2$ and $SnMe_2$ for M = Co) via ^{13}C and ^1H NMR measurements at temperatures from −130 to +150 °C revealed that all the phosphido- and arsenic-bridged iron dimers exhibit R group exchange with coalescence temperatures in the range 50–100 °C, while the $GeMe_2$- and $SnMe_2$-bridged molecules exhibit R group exchange with coalescence temperatures ca. −55 °C. Rapid site exchange of the nonequivalent carbonyl ligands was found to occur at very low temperatures in all cases, with coalescence temperatures ca. −70 °C. They concluded that no information can be obtained concerning the manner in which carbonyl ligands may be obliged to undergo site exchange during the occurrence of the R substituent exchange owing to independent carbonyl scrambling being too rapid at temperatures required for R group exchange. They also concluded that axial-equatorial R group exchange occurs simultaneously in both ligand-bridged groups but that the mechanism for this process (which may involve either bridge retention or bridge opening) remains debatable.

It is also of interest that edge-bridged binuclear metal dimers containing five-coordinate metal atoms (i.e., with no metal–

metal bond) are rare. The only other crystallographically proven examples (to our knowledge) possessing metal atoms viewed as distorted trigonal bipyramids are the chlorine-bridged $[Cu_2Cl_6(\mu_2\text{-}Cl)_2]^{4-}$ tetraanion found in the compound $[Co(en)_3]_2^{3+}[Cu_2Cl_6(\mu_2\text{-}Cl)_2]^{4-}Cl_2^-\cdot 2H_2O$,[32] the $Mo_2(OPr\text{-}i)_4(NO)_2(\mu_2\text{-}OPr\text{-}i)_2$ molecule,[33] and the isomorphous bis(*N*-methylsalicylaldiminato)metal(II) dimers of Zn(II), Co(II), and Mn(II).[34] In each of these latter pseudocentrosymmetric dimers[34] containing two oxygen-shared atoms, the equatorial sites of the distorted trigonal-bipyramidal arrangement about each metal(II) are occupied by an oxygen and two nitrogen atoms with a terminal oxygen atom and a bridging oxygen atom being located at the axial sites. The geometries of the $[Fe_2(CO)_6(\mu_2\text{-}PPh_2)_2]^{2-}$ dianion and the other above bi(trigonal-bipyramidal) metal dimers are distinctly different from that of the chlorine-bridged $[Ni_2Cl_6(\mu_2\text{-}Cl)_2]^{4-}$ tetraanion, for which Ross and Stucky[40] found that the five-coordinate nickel atoms possess an approximately square-pyramidal geometry. A crystallographic inversion center requires that the two square pyramids, which are joined along one common basal edge, have their apices pointing to opposite directions. This centrosymmetric dimeric arrangement of two square pyramids was also established by Strähle and Bärnighausen[41] from their structural determination of $V_2(NCl)_2Cl_4(\mu_2\text{-}Cl)_2$ in which the -NCl ligands occupy the axial positions. It may be presumed for these binuclear metal dimers that the energy difference between the two idealized five-coordinate metal geometries is also quite small, as was demonstrated in the case of five-coordinate mononuclear metal complexes by Raymond, Corfield, and Ibers,[42] who showed the simultaneous existence in the solid state of both geometries for the $[Ni(CN)_5]^{3-}$ trianion in $[Cr(en)_3]^{3+}[Ni(CN)_5]^{3-}\cdot 1.5H_2O$. A general theory of substituent effects and geometrical preferences in pentacoordinate transition metal complexes has been put forth by Rossi and Hoffmann.[43]

E. Steric Relationship between the Bridging PPh_2 Ligands of $[Fe_2(CO)_6(\mu_2\text{-}PPh_2)_2]^n$ (n = 0, −2). Figure 2 clearly indicates for the dianion ($n = -2$) that the magnitudes of the directional distortions of the carbonyl ligands are fixed primarily by the nonbonding interactions with the phenyl rings which themselves are seen to be twisted appreciably out of the vertical plane perpendicular to the horizontal Fe_2P_2 plane and passing through the P and P′ atoms. In contrast, it is apparent from Figure 1 of the neutral parent ($n = 0$) that the four phosphorus-attached phenyl carbon atoms of the two independent PPh_2 ligands are all close to the corresponding vertical mirror plane passing through the two phosphorus atoms and the midpoint of the Fe–Fe bond.

The large angular deformation of each of the phenyl rings (CA and CB) relative to the planar Fe_2P_2 core for $n = -2$ is also shown from the large differences found between the normally equivalent Fe-P-CA(1) and Fe′-P-CA(1) angles of 109.1 (3) and 115.0 (3)°, respectively, for ring CA and likewise between the normally equivalent Fe-P-CB(1) and Fe′-P-CB(1) angles of 119.1 (3) and 107.5 (3)°, respectively, for ring CB. Furthermore, a discernible bending of each phenyl ring from its attached phosphorus atom is evidenced from the significant variations between the P-CA(1)-CA(2) and P-CA(1)-CA(6) angles of 116.3 (7) and 124.6 (7)°, respectively, for ring CA and between the P-CB(1)-CB(2) and P-CB(1)-CB(6) angles of 119.1 (6) and 124.2 (3)°, respectively, for the other ring CB. A net consequence of these angular ring deformations is that the two phenyl rings CA and CB are oriented almost perpendicular to each other (Figure 2).

On the other hand, an examination of the corresponding angles in the neutral parent ($n = 0$) shows that the normally equivalent Fe(1)-P(n)-C(m) and Fe(2)-P(n)-C(m) angles for a given n and m value (where n = 1, 2 and m = 1, 2) differ from each other by only 0.3, 1.6, 0.7, and 0.1° for the four independent phenyl rings. Although these small variations reflect an essentially symmetrical disposition of the phosphorus-attached phenyl carbon atoms, the highly bent Fe_2P_2 core for $n = 0$ expectedly gives rise to nonequivalent equatorial and axial phenyl sites on each phosphorus atom, P(n), with the axial phenyl substituent having a significantly larger mean value for its two experimentally equivalent Fe-P(n)-C_{ax} angles than that for the two experimentally equivalent Fe-P(n)-C_{eq} angles of the equatorial phenyl substituent (viz., 123.2 (av) vs. 120.6° (av) for P(1) and 123.8 (av) vs. 119.6° (av) for P(2)). Another contrasting feature between $n = 0$ and $n = -2$ is the lack for $n = 0$ of any significant bending deformation for each of the four independent phenyl rings about its P-C bond, as indicated from the eight individual P-C-C angles of range 119–122° being within experimental error to the nondistorted value of 120°.

These comparisons are consistent with the premise that the planar Fe_2P_2 core ($\theta = 180°$) of the dianion ($n = -2$) produces a steric overcrowding of the carbonyl and phenyl groups as reflected by their large angular distortions from a symmetrical idealized geometry, in contradistinction to steric repulsions among the ligands being relatively much less in the highly bent Fe_2P_2 core ($\theta = 100°$) of the neutral parent ($n = 0$). In spite of these large angular variations of the phenyl rings between $[Fe_2(CO)_6(\mu_2\text{-}PPh_2)_2]^n$ (n = 0, −2) as well as the large difference between the observed θ angles in their Fe_2P_2 cores, there is only a small variation between the H_5C_6-P-C_6H_5 angles for $n = -2$ (101.0 (4)°) and $n = 0$ (98.7° (av)).

F. Stereochemical Relationship of $[Fe_2(CO)_6(\mu_2\text{-}PPh_2)_2]^n$ (n = 0, −2) with Related Phosphido-Bridged Dimers with and without Metal–Metal Bonds and Resulting Bonding Implications. Table V compares the mean geometrical parameters of the M_2P_2 cores not only for the $[Fe_2(CO)_6(\mu_2\text{-}PPh_2)_2]^n$ (n = 0, −2) pair but also for three other pairs of phosphido-bridged dimers with and without electron-pair metal–metal bonds. In each case there is an analogous major alteration in the geometry of the M_2P_2 core due primarily to metal–metal bond rupture, which likewise may be viewed as a structural consequence of the addition of two electrons to the LUMO of the (metal–metal)-bonded dimer. Hence, the structural evidence given here for antibonding dimetal and antibonding M-P orbital character in the LUMO of the (metal–metal)-bonded $Fe_2(CO)_6(\mu_2\text{-}X)_2$-type dimer provides further support for similar orbital character in the LUMO of the electronically equivalent and structurally analogous (Co–Co)-bonded $Co_2(\eta^5\text{-}C_5H_5)_2(\mu_2\text{-}PR_2)_2$ dimer. It is noteworthy that the corresponding (metal–metal)-nonbonded $Ni_2(\eta^5\text{-}C_5H_5)_2(\mu_2\text{-}PPh_2)_2$ dimer also bears a geometrical resemblance with the $[Fe_2(CO)_6(\mu_2\text{-}PPh_2)_2]^{2-}$ dianion in accord with the isolobal orbital nature[44] of the $Ni(C_5H_5)$ and $Fe(CO)_3^-$ fragments.

Of prime interest is that these structural and bonding trends for phosphido- and mercapto-bridged ligands parallel those established both experimentally and theoretically for the edge-bridged, bioctahedral metal carbonyl pairs, $[M_2(CO)_8(\mu_2\text{-}PR_2)_2]^n$ (where M = Cr, Mn for $n = 0$; n = 0, −2 for M = Cr; n = 0, +2 for M = Mn),[45,46] and for the edge-bridged bioctahedral metal cyclopentadienyl analogues, $[cis\text{-}Fe_2(\eta^5\text{-}C_5H_5)_2(\mu_2\text{-}PR_2)_2]^n$ (where n = +2, 0).[31,47]

$[Na(2,2,2\text{-crypt})]^+$ Monocation. The cryptate ligand (Figure 4) consists of a macrobicyclic diaminohexaether which completely encloses the sodium ion in its cavity. The heteroatom polyhedron, defined by the six oxygen and two nitrogen atoms as potential coordination sites, approximately conforms to trigonal D_3-32 symmetry and is intermediate between a bicapped trigonal prism and a bicapped trigonal antiprism. The extent of its twisting about the threefold axis through the two nitrogen atoms is given by the angle of twist α between the two

Table V. Comparison of Mean Geometrical Parameters for Pairs of Diphenylphosphido-Bridged Dimers with and without Electron-Pair Metal-Metal Bonds

dimeric pairs	ref	idealized M_2P_2 geometry	torsional angle[a] of M_2P_2 core, deg	M-M bond order	M-M, Å	M-P, Å	P···P, Å	M-P-M′, deg	P-M-P′, deg
$[Fe_2(CO)_6(\mu_2\text{-}PPh_2)_2]^n$									
$n = 0$	*b*	C_{2v} (bent)	100	1	2.623(2)	2.233(2)	2.866(3)	72.0(1)	79.9(1)
$n = 2-$ (as $[Na(2,2,2\text{-crypt})]^+$ salt)	*c*	D_{2h} (planar)	180	0	3.630(3)	2.280(3)	2.759(5)	105.5(1)	74.5(1)
$M_2(\eta^5\text{-}C_5H_5)_2(\mu_2\text{-}PPh_2)_2$									
M = Co	*d*	C_{2v} (bent)	105	1	2.56(1)	2.16(1)	2.88(2)	72.5(5)	83.7(5)
M = Ni	*d*	D_{2h} (planar)	180	0	3.36(1)	2.15(1)	2.70(1)	102.4(2)	77.6(2)
$M_2(CO)_8(\mu_2\text{-}PPh_2)_2$									
M = Cr	*e*	D_{2h} (planar)	180	1	2.911(2)	2.352(2)	3.694(2)	76.5(1)	103.5(1)
M = Mn	*e*	D_{2h} (planar)	180	0	3.693(2)	2.391(3)	3.035(3)	101.1(1)	78.8(1)
$[cis\text{-}Fe_2(\eta^5\text{-}C_5H_5)_2(CO)_2(\mu_2\text{-}PPh_2)_2]^n$									
$n = 2+$ (as $[SbF_6]^-$ salt)	*f*	C_{2v} (bent)	176	1	2.764(4)	2.236(7)	3.510(9)	76.3(2)	103.4(3)
$n = 0$	*f*	C_{2v} (bent)	168	0	3.498(4)	2.261(6)	2.839(8)	101.4(2)	77.8(2)

[a] Torsional angle between two planes in the M_2P_2 core each formed by the two bridging P atoms and one M atom. [b] Reference 6. [c] This work. [d] Reference 25. [e] Reference 45. [f] Reference 31.

equilateral oxygen triangles from the bicapped trigonal prism.

The overall geometry of the $[Na(2,2,2\text{-crypt})]^+$ cation (Figure 4) in this crystal structure is basically similar to those determined from X-ray diffraction studies[48] of other $[Na(2,2,2\text{-crypt})]^+$ salts. The dihedral angles for the cryptate ligand in this structure are listed in Table II. It was previously noted[48a] that the cryptate ligand undergoes significant twisting in order to complex the Na^+ cation which is somewhat too small for effective coordination with the two nitrogen and six oxygen atoms. In this crystal structure the determined twist angle α of 34° is intermediate between that of 45° reported[48a,d] for $[Na(2,2,2\text{-crypt})]^+I^-$ and that of 21° reported[48a,b] for the corresponding $[K(2,2,2\text{-crypt})]^+I^-$. The unusual geometrical feature encountered in this structure of the $[Na(2,2,2\text{-crypt})]^+$ cation from those of the previously reported ones[48] is the highly asymmetric coordination of the Na^+ ion to the eight heteroatoms. Whereas one of the two Na^+-N distances of 2.693 (8) Å and the six Na^+-O distances of 2.497 (7) to 2.748 (7) Å in the present structure compare favorably with the corresponding distances in other known structures, the remaining Na^+-N distance of 3.142 (8) Å, which is 0.2 Å longer than any previously reported value, reinforces the belief[48a] that its relatively low stability compared to those of the K^+ and Rb^+ ions arises from the Na^+ ion being in too large a hole.

Bonding and Stereochemical Implications. This structural investigation has established that a two-electron reduction of $Fe_2(CO)_6(\mu_2\text{-}PPh_2)_2$, a representative member of the $Fe_2(CO)_6(\mu_2\text{-}X)_2$ series (X = PR_2, AsR_2, SR, SeR, and other electronically equivalent ligands), will produce cleavage of the electron-pair Fe-Fe bond to give a dianion comprised of two distorted trigonal bipyramids sharing a common axial-equatorial edge. This dramatic geometrical change, involving a 1.01 Å increase in the Fe-Fe distance from a bonding value of 2.623 (2) Å in the parent molecule to a nonbonding value of 3.630 (3) Å in the dianion, provides the first direct experimental evidence that the LUMOs of these particular dimers possess large antibonding dimetal orbital character in complete accord with the MO investigation by Teo et al.[7] of selected $Fe_2(CO)_6X_2$ complexes via the parameter-free Fenske-Hall model.[49] Moreover, these results are in harmony with the spectroscopic NMR, ESR, Mössbauer, and IR data obtained by Dessy and co-workers[29] for the $[Fe_2(CO)_6(\mu_2\text{-}PMe_2)_2]^n$ dimers ($n = 0, -1, -2$) and analyzed by Teo et al.[7] on the basis of their MO calculations.

A concomitant lengthening of 0.05 Å in the mean value of the Fe-P bonds was also found upon reduction of the diphenylphosphido-bridged dimer to the dianion. This relatively small but yet significant change supports the premise that the LUMO in the neutral parent likewise has significant antibonding Fe-P orbital character. The Fenske-Hall-type MO calculations do not show substantial bridging ligand character in either the HOMOs or the LUMOs of the selected neutral $Fe_2(CO)_6X_2$ complexes (where X_2 denotes $(SCH_3)_2$, $(PH_2)_2$, S_2, and $CH_3N{=}NCH_3$). However, from subsequent Hückel MO calculations Burdett[17] emphasized the different antibonding Fe-P interactions as well as bonding Fe-Fe interactions in the HOMOs in rationalizing the observed variation between the molecular geometry of the neutral $P(CF_3)_2$-bridged dimer and those with phosphorus-attached H, Me, or Ph substituents. Burdett[17] also commented that, because the LUMO of a neutral phosphido-bridged dimer, in general, has both antibonding Fe-P and antibonding Fe-Fe orbital character, its occupation upon reduction should increase the torsional angle of the Fe_2P_2 core from a bent toward a planar geometry in order to decrease both Fe-P and Fe-Fe repulsions. In this connection, it is noteworthy that previous Fenske-Hall-type calculations by Teo et al.[46] do show not only for the $(Mn_2(CO)_8(\mu_2\text{-}PR_2)_2]^n$ series ($n = +2, +1, 0$) but also for the electronically equivalent $[Cr_2(CO)_8(\mu_2\text{-}PR_2)_2]^n$ series ($n = 0, -1, -2$) that the LUMOs of the (Mn-Mn)-bonded dimanganese dimer for $n = +2$ and of the (Cr-Cr)-bonded dichromium dimer for $n = 0$ contain significant antibonding M-P character such that a weakening of M-P bonds is expected upon reduction. This predicted trend is also in agreement with total M-P overlap populations which for both series show a definite stepwise decrease upon reduction.[46]

While recognizing the indicated electronic influence of the metal-ligand interactions, we wish to emphasize that both the experimental and theoretical results indicate that the "net" metal-metal interactions represent the primary driving force in producing the resultant overall changes in molecular geometry for the dimeric species presented in Table V. Based upon a consideration of only the metal-metal interactions whose energy-level ordering is governed by the nature of the metal-ligand interactions,[50] a qualitative metal cluster model[46b,51] has been utilized for transition-metal dimers, trimers, and tetramers in correlating variations in geometry with changes in electronic configuration. The successful application of this symmetry-based model to a given ligand-bridged metal cluster, which maintains an architectural integrity without bond rupture during its gain and/or loss of electrons, depends

upon two major boundary conditions being satisfied. First, the ligands of the metal cluster must be "sterically innocent" such that electronic effects dominate over steric effects in giving rise to an equilibrium geometry. Second, the assumed separability of the metal–metal interactions from the metal–ligand interactions necessitates that the metal–ligand interactions be much stronger than the metal–metal interactions (i.e., the metal–ligand bonds must be relatively stiff compared to the metal–metal bonds which, although being much weaker, are still sufficiently strong to produce definite geometrical perturbations which may be detected from structural studies). Table V illustrates for diphenylphosphido ligands (or other analogously covalently linked ligands of sufficient metal–ligand bond strength) that the large change in molecular architecture caused by an addition of two electrons either from reduction or from a change of metal atoms is accompanied by only small, symmetrical bond-length variations in the metal–(bridging ligand) bonds. It is apparent that the metal–ligand bonds must be sufficiently strong to prevent large, unsymmetrical variations in the metal–ligand bond lengths, such as occur for the copper and silver halide cluster systems.[52]

The determined planarity of the Fe_2P_2 core in the $[Fe_2(CO)_6(\mu_2\text{-}PPh_2)_2]^{2-}$ dianion points to the definite possibility that the Fe_2P_2 core in the dimethylphosphido-bridged dianion is likewise planar and not bent as proposed by Dessy and co-workers[29] from their ^1H NMR spectral measurements. Based upon the premise that the configuration of the dimethylphosphido-bridged dianion is indeed analogous to that observed in the solid state for the diphenylphosphido-bridged dianion, it follows that the spectroscopic determination[29] in solution of two structurally different kinds of methyl substituents (which undergo site exchange at sufficiently high temperature) may instead reflect their unsymmetrical disposition relative to a planar Fe_2P_2 core as was found for the phenyl substituents in the $[Fe_2(CO)_6(\mu_2\text{-}PPh_2)_2]^{2-}$ dianion. Furthermore, it is noteworthy that the dimethylphosphido-bridged dianion containing five-coordinate iron atoms has a lower coalescence temperature of −66 (2) °C[29] for methyl site exchange than that of +74 (3) °C[39] for its corresponding neutral parent containing six-coordinate iron atoms. In fact, the pseudorotation mechanism proposed by Adams and Cotton[38] for the axial–equatorial methyl group exchange in the (Co–Co)-bonded $Co_2(CO)_6(\mu_2\text{-}GeMe_2)_2$ analogue of the neutral dimethylphosphido-bridged iron dimer presumably requires that their proposed planar intermediate (or transition-state) species with trigonal-bipyramidal iron atoms have C_{2h} symmetry.[53] Its near conformity to the previously described C_{2h}-distorted geometry determined in the solid state for the $[Fe_2(CO)_6(\mu_2\text{-}PPh_2)_2]^{2-}$ dianion provides support for the methyl site exchange found[39] in the (M–M)-bonded $M_2(CO)_6(\mu_2\text{-}EMe_2)_2$ dimers (M = Fe, E = P, As; M = Co, E = Ge, Sn) occurring via the proposed Adams–Cotton pseudorotation mechanism[38] with non-(bridge opening).

Acknowledgments are gratefully made for the support of this research by J.P.C. to the National Science Foundation (CHE 75-17018) and by L.F.D. to the National Science Foundation (CHE 77-24309).

Supplementary Material Available: A listing of the observed and calculated structure factors (21 pages). Ordering information is given on any current masthead page.

References and Notes

(1) (a) University of Wisconsin—Madison; (b) Stanford University; (c) Eastman Kodak Co., Rochester, N.Y.; (d) Department of Chemistry, University of Oregon.

(2) (a) J. P. Collman, R. K. Rothrock, R. G. Finke, and F. Rose-Munch, *J. Am. Chem. Soc.*, **99**, 7381 (1977); (b) R. K. Rothrock, Ph.D. Thesis, Stanford University, 1978.

(3) R. C. Ryan, C. U. Pittman, and J. P. O'Connor, *J. Am. Chem. Soc.*, **99**, 1986 (1977).

(4) R. C. Ryan and L. F. Dahl, *J. Am. Chem. Soc.*, **97**, 6904 (1975).

(5) R. Poilblanc, *Nouveau J. Chim.*, **2**, 145 (1978).

(6) J. R. Huntsman, Ph.D. Thesis, University of Wisconsin—Madison, 1973.

(7) B.-K. Teo, M. B. Hall, R. F. Fenske, and L. F. Dahl, *Inorg. Chem.*, **14**, 3103 (1975).

(8) (a) R. W. Broach, CARESS, "A FORTRAN Diffractometer Data-Reduction Program", Ph.D. Thesis, University of Wisconsin—Madison, 1977; (b) J. C. Calabrese, SORTMERGE, "A Data-Merging and Decay-Correction Program", Ph.D. Thesis (Appendix I), University of Wisconsin—Madison, 1971; (c) J. F. Blount, DEAR, "An Absorption-Correction Program", 1965; (d) P. Main, L. Lessinger, M. M. Woolfson, G. Germain, and J.-P. Declercq, MULTAN 76; (e) J. C. Calabrese, MAP, "A Local FORTRAN Fourier Summation and Molecular Assemblage Program", 1972; (f) J. C. Calabrese, "A Crystallographic Variable Matrix Least-Squares Program", University of Wisconsin—Madison, 1972; (g) J. C. Calabrese, MIRAGE, Ph.D. Thesis (Appendix III), University of Wisconsin—Madison, 1971; (h) ORFLSR, "A Local Rigid-Body Least-Squares Program", adapted from the Busing–Martin–Levy ORFLS, ORNL-TM-305, Oak Ridge National Laboratory, Oak Ridge, Tenn., 1963; (i) W. R. Busing, K. O. Martin, and H. A. Levy, ORFFE, ORNL-TM-306, Oak Ridge National Laboratory, Oak Ridge, Tenn., 1964; (j) D. L. Smith, "A Least-Squares Planes Program", Ph.D. Thesis (Appendix IV), University of Wisconsin—Madison, 1962; (k) C. K. Johnson, ORTEP-II, 1970.

(9) (a) "International Tables for X-ray Crystallography," Vol. III, Kynoch Press, Birmingham, England, 1962, pp 161–165; (b) D. T. Cromer and J. B. Mann, *Acta Crystallogr., Sect. A*, **24**, 321 (1968); (c) R. F. Stewart, E. R. Davidson, and W. T. Simpson, *J. Chem. Phys.*, **42**, 3175 (1965); (d) D. T. Cromer and D. Liberman, *ibid.*, **53**, 1891 (1970).

(10) G. Germain, P. Main, and M. M. Woolfson, *Acta Crystallogr., Sect. A*, **27**, 368 (1971).

(11) The unweighted and weighted discrepancy factors used are $R_1 = [\sum \| F_o| - |F_c \| / \sum |F_o|] \times 100$ and $R_2 = [\sum w_i \| F_o| - |F_c\|^2 / \sum w_i |F_o|^2]^{1/2} \times 100$. All least-squares refinements were based on the minimization of $\sum w_i \| F_o| - |F_c\|^2$ with individual weights of $w_i = 1/\sigma^2(F_o)$ assigned on the basis of the esd's[8a] of the observed structure factors.

(12) L. F. Dahl and C. H. Wei, *Inorg. Chem.*, **2**, 328 (1963).

(13) C. H. Wei and L. F. Dahl, *Inorg. Chem.*, **4**, 1 (1965).

(14) L. F. Dahl, J. D. Sinclair, and B. K. Teo in "The Organic Chemistry of Iron", E. A. Koerner von Gustorf, Ed., Academic Press, New York.

(15) W. Clegg, *Inorg. Chem.*, **15**, 1609 (1976).

(16) G. Le Borgne, D. Grandjean, R. Mathieu, and R. Poilblanc, *J. Organomet. Chem.*, **131**, 429 (1977).

(17) J. K. Burdett, *J. Chem. Soc., Dalton Trans.*, 423 (1977).

(18) W. Hieber and P. Spacu, *Z. Anorg. Allg. Chem.*, **233**, 353 (1937).

(19) W. Schweckendieck, German Patent 1 072 244 (Dec 1959).

(20) R. G. Hayter, *J. Am. Chem. Soc.*, **86**, 823 (1964).

(21) C. H. Wei and L. F. Dahl, *J. Am. Chem. Soc.*, **90**, 3969 (1968).

(22) C. H. Wei and L. F. Dahl, *Inorg. Chem.*, **6**, 1229 (1967).

(23) Also isolated from our reaction[6] of $Co_2(CO)_8$ and tetraphenylbiphosphine was the previously unreported dark green $Co_3(CO)_6(\mu_2\text{-}PPh_2)_3$ trimer, which was found from an X-ray crystallographic analysis[6] to consist of a completely bonding isosceles triangle of cobalt atoms with edge-bridged diphenylphosphido ligands.

(24) A similar conclusion was also reached by Professor H. Vahrenkamp of the University of Freiburg, West Germany (private communication to L. F. Dahl, Sept 1978).

(25) J. M. Coleman and L. F. Dahl, *J. Am. Chem. Soc.*, **89**, 542 (1967).

(26) R. G. Hayter, *Inorg. Chem.*, **2**, 1031 (1963); R. G. Hayter and L. F. Williams, *J. Inorg. Nucl. Chem.*, **26**, 1977 (1964).

(27) R. E. Dessy, R. Kornmann, C. Smith, and R. G. Hayter, *J. Am. Chem. Soc.*, **90**, 2001 (1968).

(28) R. E. Dessy and L. Wieczorek, *J. Am. Chem. Soc.*, **91**, 4963 (1969).

(29) (a) R. E. Dessy, A. L. Rheingold, and G. D. Howard, *J. Am. Chem. Soc.*, **94**, 746 (1972); (b) R. E. Dessy and L. A. Bares, *Acc. Chem. Res.*, **5**, 415 (1972).

(30) (a) L. F. Dahl, R. Rodulfo de Gil, and R. D. Feltham, *J. Am. Chem. Soc.*, **91**, 1653 (1969); (b) N. G. Connelly and L. F. Dahl, *ibid.*, **92**, 7472 (1970).

(31) (a) J. D. Sinclair, Ph.D. Thesis, University of Wisconsin—Madison, 1972; (b) J. D. Sinclair, N. G. Connelly, and L. F. Dahl, submitted for publication.

(32) D. J. Hodgson, P. K. Hale, and W. E. Hatfield, *Inorg. Chem.*, **10**, 1061 (1971).

(33) M. H. Chisholm, F. A. Cotton, M. W. Extine, and R. L. Kelly, *J. Am. Chem. Soc.*, **100**, 3354 (1978).

(34) P. L. Orioli, M. Di Vaira, and L. Sacconi, *Inorg. Chem.*, **5**, 400 (1966).

(35) Cf. J. B. Headridge, "Electrochemical Techniques for Inorganic Chemists", Academic Press, New York, 1969, p 97.

(36) The importance of steric effects of phosphorus ligands to structures, spectroscopic properties, and chemical behavior of metal complexes is presented in an excellent, comprehensive review: C. A. Tolman, *Chem. Rev.*, **77**, 313 (1977).

(37) Cf. (a) R. S. Berry, *J. Chem. Phys.*, **32**, 933 (1960); (b) G. M. Whitesides and H. L. Mitchell, *J. Am. Chem. Soc.*, **91**, 5384 (1969); (c) K. E. DeBruin, K. Naumann, G. Zon, and K. Mislow, *ibid.*, **91**, 7031 (1969); (d) I. Ugi, D. Marquarding, H. Klusacek, P. Gillespie, and F. Ramirez, *Acc. Chem. Res.*, **4**, 288 (1971); (e) R. R. Holmes, *ibid.*, **5**, 296 (1972); (f) J. R. Shapley and J. A. Osborn, *ibid.*, **6**, 305 (1973).

(38) R. D. Adams and F. A. Cotton, *J. Am. Chem. Soc.*, **92**, 5003 (1970).

(39) R. D. Adams, F. A. Cotton, W. R. Cullen, D. L. Hunter, and L. Mihichuk, *Inorg. Chem.*, **14**, 1395 (1975).

(40) F. K. Ross and G. D. Stucky, *J. Am. Chem. Soc.*, **92**, 4538 (1970).

(41) J. Strähle and H. Bärnighausen, *Z. Anorg. Allg. Chem.*, **357**, 325 (1968).

(42) K. N. Raymond, P. W. R. Corfield, and J. A. Ibers, *Inorg. Chem.*, **7**, 1362 (1968).

(43) A. R. Rossi and R. Hoffmann, *Inorg. Chem.*, **14**, 365 (1975).

(44) J. W. Lauher and R. Hoffmann, *J. Am. Chem. Soc.*, **98**, 1729 (1976).

(45) J. R. Huntsman, J. C. Compton, R. S. Gall, and L. F. Dahl, unpublished re-

search.
(46) (a) B.-K. Teo, M. B. Hall, R. F. Fenske, and L. F. Dahl, *J. Organomet. Chem.*, **70**, 413 (1974); (b) B.-K. Teo, Ph.D. Thesis, University of Wisconsin—Madison, 1973.
(47) C. F. Campana, Ph.D. Thesis, University of Wisconsin—Madison, 1975, C. F. Campana and L. F. Dahl, to be published.
(48) (a) B. Metz, D. Moras, and R. Weiss, *Chem. Commun.*, 444 (1971); (b) D. Moras, B. Metz, and R. Weiss, *Acta Crystallogr., Sect. B*, **29**, 383 (1973); (c) *ibid.*, **29**, 388 (1973); (d) D. Moras and R. Weiss, *ibid.*, **29**, 396 (1973); (e) *ibid.*, **29**, 400 (1973); (f) F. J. Tehan, B. L. Barnett, and J. L. Dye, *J. Am. Chem. Soc.*, **96**, 7203 (1974); (g) D. G. Adolphson, J. D. Corbett, and D. J. Merryman, *ibid.*, **98**, 7234 (1976); (h) R. G. Teller, R. G. Finke, J. P. Collman, H. B. Chin, and R. Bau, *ibid.*, **99**, 1104 (1977).
(49) (a) M. B. Hall and R. F. Fenske, *Inorg. Chem.*, 11, 768 (1972); (b) R. F. Fenske, *Pure Appl. Chem.*, **27**, 61 (1971); (c) *Prog. Inorg. Chem.*, **21**, 179 (1976).
(50) Cf. R. S. Gall, C. Ting-Wah Chu, and L. F. Dahl, *J. Am. Chem. Soc.*, **96**, 4019 (1974).
(51) Cf. Trinh-Toan, B.-K. Teo, J. A. Ferguson, T. J. Meyer, and L. F. Dahl, *J. Am. Chem. Soc.*, **99**, 408 (1977), and references cited therein.
(52) Cf. (a) Boon-Keng Teo and J. C. Calabrese, *J. Am. Chem. Soc.*, **97**, 1256 (1975); (b) *Inorg. Chem.*, **15**, 2467, 2474 (1976); (c) M. R. Churchill, J. Donahue, and F. J. Rotella, *ibid.*, **15**, 2752 (1976); (d) M. R. Churchill, B. G. DeBoer, and S. J. Mendak, *ibid.*, **14**, 2041 (1975); (e) M. R. Churchill, B. G. DeBoer, and D. J. Donovan, *ibid.*, **14**, 617 (1975).
(53) W. G. Klemperer, *J. Am. Chem. Soc.*, **94**, 8360 (1972).

Demonstration of the Generality of the $[Fe_4S_4(SR)_4]^{2-}$ (Compressed D_{2d})/$[Fe_4S_4(SR)_4]^{3-}$ (Elongated D_{2d}) Structural Change in Electron-Transfer Reactions of Ferredoxin 4-Fe Site Analogues. A Model for Unconstrained Structural Changes in Ferredoxin Proteins

Edward J. Laskowski,[1a] John G. Reynolds,[1a] Richard B. Frankel,*[1b] S. Foner,[1b] G. C. Papaefthymiou,[1b] and R. H. Holm*[1a]

Contribution from the Department of Chemistry, Stanford University, Stanford, California 94305, and the Francis Bitter National Magnet Laboratory, Massachusetts Institute of Technology, Cambridge, Massachusetts 02139.
Received April 4, 1979

Abstract: The ^{57}Fe Mössbauer, magnetic susceptibility, magnetization, and EPR properties of an extensive series of $(R_4'N)_3[Fe_4S_4(SR)_4]$ compounds (R = Ph, *o*-, *m*-, *p*-C_6H_4Me, *p*-C_6H_4-*i*-Pr, CH_2Ph, CH_2-*p*-C_6H_4OMe) have been examined in the solid state and in frozen acetonitrile solutions. The cluster trianions serve as analogues of the sites of Fd_{red} proteins. Based on similarities and differences in their properties in the solid state the compounds divide into two categories: those whose $[Fe_4S_4(SR)_4]^{3-}$ clusters contain tetragonal or nontetragonal Fe_4S_4 core structures. The lack of core structural uniformity is attributed to perturbing influences in the solid state. Irrespective of their solid-state category all compounds in frozen solution exhibit essentially coincident properties (most thoroughly documented by EPR and Mössbauer spectral results), which are indicative of a single core structure of a set of closely related core structures. From a previous demonstration of the similarity of properties of $[Fe_4S_4(SPh)_4]^{3-}$ salts in the solid and solution state and the X-ray structure of this cluster, the solution core structure of the set of cluster trianions is identified as elongated tetragonal. These findings, together with the previously established high degree of core structural uniformity in the Fd_{ox} analogues $[Fe_4S_4(SR)_4]^{2-}$, provide substantial experimental support for two proposals: (1) an elongated (idealized) D_{2d} core structure is the intrinsically stable configuration of $[Fe_4S_4(SR)_4]^{3-}$; (2) the unconstrained idealized core structural change accompanying electron transfer is $[Fe_4S_4(SR)_4]^{2-}$ (compressed D_{2d}) $\rightleftharpoons$ $[Fe_4S_4(SR)_4]^{3-}$ (elongated D_{2d}). This process serves as a representation of protein site structural changes in a Fd_{ox}/Fd_{red} electron transfer couple in the absence of extrinsic constraints such as might be imposed by protein structural features.

Introduction

Previous experiments have firmly established the following isoelectronic relationships between the $[Fe_4S_4(S\text{-}Cys)_4]$ sites in ferredoxin (Fd) proteins and synthetic clusters: $Fd_{ox} \equiv [Fe_4S_4(SR)_4]^{2-}$,[2,3] $Fd_{red} \equiv [Fe_4S_4(SR)_4]^{3-}$.[3-6] Following the earlier synthesis of the cluster dianions,[2,3,7] the recent preparation of cluster trianions[4] has provided access to analogues of the sites of both members of the Fd_{ox}/Fd_{red} redox couple, which has been implicated in electron-transport chains to numerous oxidoreductase enzymes.[8] Further, there is substantial evidence in some cases (e.g., trimethylamine dehydrogenase,[9] hydrogenase,[10] FeMo proteins of nitrogenase[11]) and a definite possibility with other Fe–S enzymes[8] that one or more Fe_4S_4 units are contained within the enzyme structure and, in such instances, may function in internal electron transfer to and from catalytic sites. An ultimately satisfactory interpretation of the operation of any biological redox site, in terms of its rates and potentials of electron transfer, minimally requires accurate structural definition of the site in both oxidation levels of the redox couple in question. Although the structures of *Peptococcus aerogenes* Fd_{ox}[12] (two Fe_4S_4 units) and the reduced *Chromatium* "high-potential" protein[12b,c] (HP_{red}, one Fe_4S_4 unit isoelectronic with those in Fd_{ox}) have been solved to 2 Å resolution, there is at present no structural data from X-ray diffraction on any Fd_{red} protein. Very recent EXAFS studies[13] have verified the close structural similarity between Fd_{ox}, HP_{red}, and $[Fe_4S_4(SR)_4]^{2-}$, consistent with results from diffraction investigations,[2,7,12] and have revealed small changes (<0.1 Å) in mean Fe–S and Fe · · · Fe distances in the two oxidation levels of a bacterial Fd. However, this method is insufficiently precise to localize the small structural differences observed.

Our approach to elucidation of structures of and structural differences between 4-Fe redox sites is based on the use of the synthetic analogues $[Fe_4S_4(SR)_4]^{2-,3-}$; pertinent findings are summarized in Figure 1. The Fd_{ox} site analogues $[Fe_4S_4(SR)_4]^{2-}$ (R = CH_2Ph,[7] Ph[14]), with the $[Fe_4S_4]^{2+}$ *core*

0002-7863/79/1501-6562$01.00/0